Electronic Supplementary Material (ESI) for Chemical Science.
This journal is © The Royal Society of Chemistry 2020

Supporting Information for

Structure and redox tuning of gas adsorption properties in calixarene-supported Fe(II)-based porous cages

Meaghan M. Deegan,[a] Tonia S. Ahmed,[b] Glenn P. A. Yap,[a] and Eric D. Bloch[a]

[a] Department of Chemistry and Biochemistry, University of Delaware, Newark, DE 19716, USA

[b] Department of Chemistry and Chemical Biology, Harvard University, 12 Oxford Street, Cambridge, MA 02138, USA

Contents:

1. Experimental Details

1.1 General Considerations.

Syntheses and manipulations of Fe-containing materials were carried out using standard Schlenk and glovebox techniques unless otherwise specified. Anhydrous EtOH was purchased from Sigma-Aldrich and stored in a glovebox over molecular sieves prior to use. $CHCl_3$ was degassed by three freeze-pump-thaw cycles and stored under N_2 in a sealed Schlenk tube prior to use. All other solvents were deoxygenated by thoroughly sparging with Ar and dried on a solvent purification system (SPS) by SG Water, USA LLC. Solvents were stored in a glovebox over molecular sieves once removed from the SPS. Other reagents were purchased from commercial vendors and used without further purification unless specified. The thiacalix[4]arene (tc4a), sulfonylcalix[4]arene ligand (sc4a), and tatb ligands were synthesized with minor modifications from previously reported synthetic protocols.[1,2,3,4,5]

1.2 Physical Methods.

Gas Adsorption Measurements

Low-pressure gas adsorption measurements were obtained on a Micromeritics Tristar II PLUS, a Micromeritics Tristar 3000, or a Micromeritics 3Flex. High-pressure methane adsorption was measured with a PCT Pro-2000 Volumetric Adsorption Analyzer. Following Et_2O exchange, solvent was decanted and residual solvent was removed to obtain cage materials as free flowing powders. Samples were activated under vacuum at a temperature optimized for each material (see below) using a Micromeritics 3Flex Degas Station over two days.

IR Spectroscopy

IR spectra were obtained on a Bruker ALPHA II ATR-IR spectrometer with OPUS data processing software. Samples were transferred from an inert atmosphere glovebox immediately prior to measurements, which were carried out in air.

Mössbauer Spectroscopy

Zero-field ^{57}Fe Mössbauer spectra of samples restrained with Paratone-N oil were collected at 90 K. The data were measured with a constant acceleration spectrometer (SEE Co., Minneapolis, MN). Isomer shifts are given relative to α-Fe metal at 298 K. Data were analyzed using an in-house package written by E. R. King in Igor Pro (Wavemetrics).

Thermogravimetric Analysis

Thermogravimetric analysis measurements were obtained using a TA Q5000 SA under N_2 flow. Samples were transferred from an inert atmosphere glovebox and loaded onto a tared aluminum pan immediately prior to initiating measurements. During the course of the measurements, samples were heated from room temperature to 600 °C at a rate of 2 °C per minute.

(1) H. Kumagai, M. Hasegawa, S. Miyanari, Y. Sugawa, Y. Sato, T. Hori, S. Ueda, H. Kamiyama and S. Miyano, *Tetrahedron Lett.*, 1997, **38**, 3971-3972.
(2) N. Iki, C. Kabuto, T. Fukushima, H. Kumagai, H. Takeya, S. Miyanari, T. Miyashi and S. Miyano, *Tetrahedron*, 2000, **56**, 1437-1443.
(3) M. H. Patel, V. B. Patel and P. S. Shrivastav, *Tetrahedron Lett.*, 2008, **49**, 3087-3091.
(4) N. Morohashi, N. Iki, A. Sugawara and S. Miyano, *Tetrahedron*, 2001, **57**, 5557-5563.
(5) L. Zou, D. Feng, T.-F. Liu, Y.-P. Chen, S. Yuan, K. Wang, X. Wang, S. Fordham, H.-C. Zhou, *Chem. Sci.*, 2016, **7**, 1063-1068.

Powder X-Ray Diffraction Measurements

Powder X-Ray diffraction measurements were obtained at the University of Delaware Advanced Materials Characterization Laboratory using a Bruker D8 X-ray diffractometer with a LynxEye detector and Cu Kα radiation (λ = 1.54 Å). All samples were loaded into 1.5 mm capillaries in a glovebox and sealed with paraffin wax under an inert atmosphere prior to measurement.

Single-Crystal X-Ray Diffraction Measurements

Crystals were mounted in viscous oil or directly in solvent ((sc4a)Fe(bdc)) onto a plastic mesh and cooled to the collection temperature. Data collection was carried out using a Bruker-AXS APEX II DUO CCD diffractometer with Cu-Kα radiation. Structures were solved using SHELXT and refined against F^2 on all data by a full-matrix least squares with SHELXL. Sample specific parameters and structure refinement details are provided below.

1.2 Synthetic Procedures

Synthesis of (sc4a)Fe(OAc): Synthesis of this Fe cluster was adapted from a published protocol for the synthesis of structurally-related Mn, Co, and Ni clusters.[6] Anhydrous $Fe(OAc)_2$ (137.2 mg, 5 equiv) and sc4a (100 mg, 1 equiv) were combined in a 1:1 mixture of $CHCl_3$/MeOH and heated to reflux for 3 h. The resultant mixture was cooled to room temperature and the solvent was removed *in vacuo*. The resultant tan powder was dissolved in a minimum of DMF (3 mL) and added to a suspension of TMABr (36.3 mg, 2 equiv) in EtOH (9 mL). The mixture was stirred overnight, generating a suspension of fine orange powder in a pale-yellow solution. This mixture was filtered and the solid was dissolved in a minimum of DMF. Layering the DMF solution with MeOH allows for isolation of the product as a highly crystalline solid. When isolated in this form, this material exhibited minimal solubility in typical organic solvents.

Synthesis of (sc4a)Fe(btc): Anhydrous $FeCl_2$ (150 mg) and sc4a (250 mg) were combined in DMF (10 mL) and heated at 100 °C overnight. After cooling to room temperature, a solution of trimesic acid (62 mg) in DMF (2 mL) was added and the solution was heated for an additional 8 h at 100 °C. The resultant solution was cooled to room temperature and diluted to a 25% EtOH solution (16 mL total). This mixture was heated overnight at 100 °C with product precipitating as large, orange crystals. This solid was washed with DMF over 2 d, with the solvent replenished with neat DMF every 10 h. Subsequently, the solids were exchanged with Et_2O over 2 d, with the solvent replenished with neat Et_2O every 10 h. Et_2O was decanted and materials were evacuated at room temperature to give powders. Samples for gas adsorption were subsequently evacuated at 175 °C (ramp rate 0.3 °C) over the course of 2 d.

Synthesis of (sc4a)Fe(bdc): Anhydrous $FeCl_2$ (150 mg) and sc4a (250 mg) were combined in DMF (8 mL) and heated at 100 °C overnight. A solution of terephthalic acid (70 mg) in DMF (2 mL) was added and the solution was heated for an additional 8 h at 100 °C. The resultant solution was cooled to room temperature and diluted to a 50% EtOH solution (20 mL total). This mixture was heated overnight at 100 °C and remained homogenous upon cooling to room temperature. Layering this solution with an equal volume of EtOH and allowing the samples to stand at room temperature led to the precipitation of the product as a dark orange crystalline solid over a couple of days. This solid was washed with DMF over 2 d, with the solvent replenished with neat DMF every 10 h. The (sc4a)Fe(bdc) cage has some DMF solubility, so the amount of DMF used was controlled (~5 mL per wash) to minimize loss of material. Subsequently, the solids were exchanged with Et_2O over 2 d, with the solvent replenished

(6) T. Kajiwara, T. Kobashi, R. Shinagawa, T. Ito, S. Takaishi, M. Yamashita and N. Iki, *Eur. J. Inorg. Chem.*, 2006, 1765-1770.

with neat Et_2O every 10 h. Et_2O was decanted and materials were evacuated at room temperature to give powders. Samples for gas adsorption were subsequently evacuated at 175 °C (ramp rate 0.3 °C) over the course of 2 d.

Synthesis of (sc4a)Fe(tatb): Anhydrous $FeCl_2$ (150 mg) and sc4a (250 mg) were combined in DMF (8 mL) and heated at 100 °C overnight. A solution of tatb (137 mg) in DMF (2 mL) was added and the solution was heated for an additional 8 h at 100 °C. The resultant solution was cooled to room temperature and diluted to a 50% EtOH solution (20 mL total). This mixture was heated overnight at 100 °C with the product precipitating as an orange crystalline solid. This solid was washed with DMF over 2 d, with the solvent replenished with neat DMF every 10 h. Subsequently, the solids were exchanged with Et_2O over 2 d, with the solvent replenished with neat Et_2O every 10 h. Et_2O was decanted and materials were evacuated at room temperature to give powders. Samples for gas adsorption were subsequently evacuated at 125 °C (ramp rate 0.2 °C) over the course of 2 d.

Synthesis of (tc4a)Fe(btc): Anhydrous $FeCl_2$ (140.6 mg), tc4a (200 mg), and trimesic acid (87.4 mg) were combined in DMF (20 mL) in a 50 mL teflon sealed Schlenk tube. The mixture was heated at 130 °C over 3 d, forming a homogeneous solution. After cooling to room temperature, the solution was filtered to remove a dark impurity and the filtrate was diluted with EtOH to a 1:1 DMF/EtOH mixture. The resultant solutions were heated at 100 °C over 2 d, with some precipitation of the product as a bright yellow crystalline solid observed. Cooling the reaction mixtures to room temperature and then further to -30 °C overnight led to the precipitation of additional product. This solid was washed with DMF over 2 d, with the solvent replenished with neat DMF every 10 h. The (tc4a)Fe(btc) cage has some DMF solubility, so the amount of DMF used was controlled (~5 mL per wash) to minimize loss of material. Subsequently, the solids were exchanged with Et_2O over 2 d, with the solvent replenished with neat Et_2O every 10 h. Et_2O was decanted and materials were evacuated at room temperature to give powders. Samples for gas adsorption were subsequently evacuated at 175 °C (ramp rate 0.3 °C) over the course of 2 d.

Chemical Oxidation of (sc4a)Fe(btc): A solution of magic blue (6-24 equiv; 75-300 mg) in MeCN (12 mL) was added to a stirred suspension of (sc4a)Fe(btc) cage (150 mg; 15% Et_2O by mass (TGA)) in MeCN (5 mL). After stirring at room temperature for 1 h, samples were centrifuged, and the solution was decanted. The resultant brown solids were washed with MeCN until the washings were nearly colorless (typically 3x, solvent exchanged every 10 h) and then solvent exchanged with Et_2O over two days, with solvent replenished every 10 h. For sample activation, the Et_2O was decanted and the samples were evacuated at room temperature until they could be manipulated as free flowing powders. For samples treated with 6 or 12 equiv of magic blue, the materials were activated under vacuum over 2 d at 175 °C (ramp rate of 0.3 °C/min). Samples treated with 18 or 24 equiv of magic blue were activated at room temperature under vacuum over the course of 2 d.

Synthesis of PCN-9 Fe: This material has been previously been prepared according to a distinct synthetic protocol.[7] A solution of tatb (200 mg) and $FeCl_2$ were combined in DMF (18 mL) and heated at 100 °C for 3 d. After cooling to room temperature, EtOH (2 mL) was added and the solution was subsequently heated for an additional 2 d, with the product precipitating as a dark red polycrystalline solid.

(7) S. Ma, D. Yuan, J.-S. Chang and H.-C. Zhou, *Inorg. Chem.*, 2009, **48**, 5398-5402.

2. Gas Adsorption

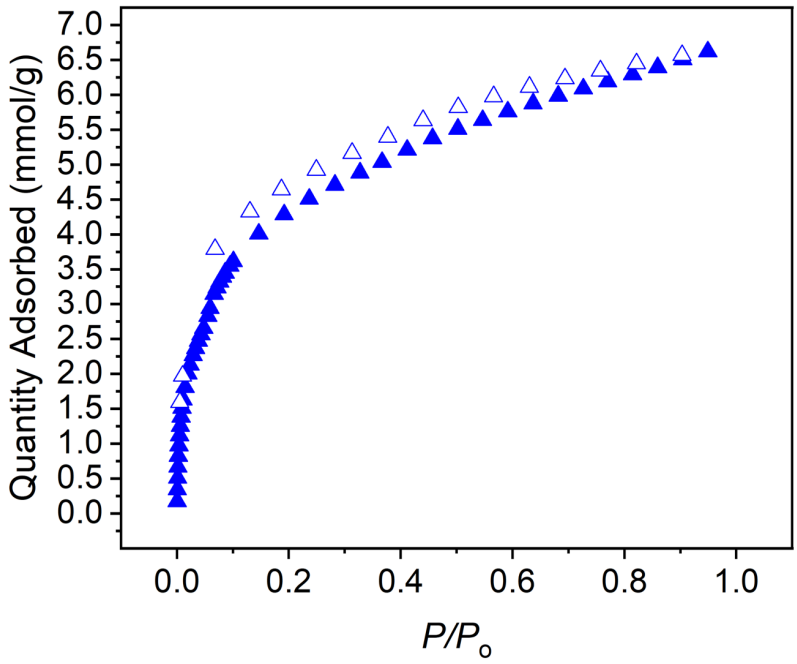

Figure S2.1. CO_2 adsorption (closed triangles) and desorption (open triangles) measured at 195 K for the (sc4a)Fe(btc) cage.

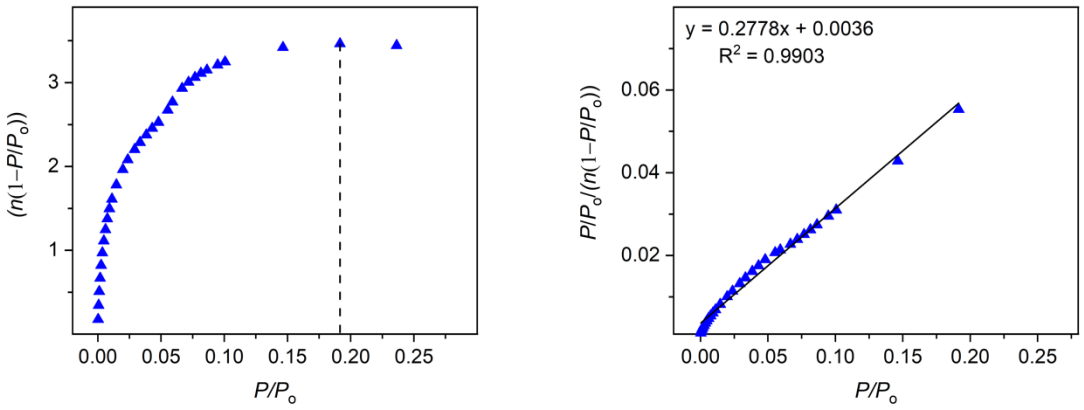

Figure S2.2. Left: Plot of n(1-P/P_0) vs. P/P_0 to determine the maximum P/P_0 used in the BET linear fit according to the first BET consistency criterion for CO_2 adsorption at 195 K for the (sc4a)Fe(btc) cage. Right: The slope of the best fit line for $P/P_0 < 0.192$ is 0.2778 and the y-intercept is 0.0036, which satisfies the second BET consistency criterion. This results in a measured surface area of 368 m^2/g.

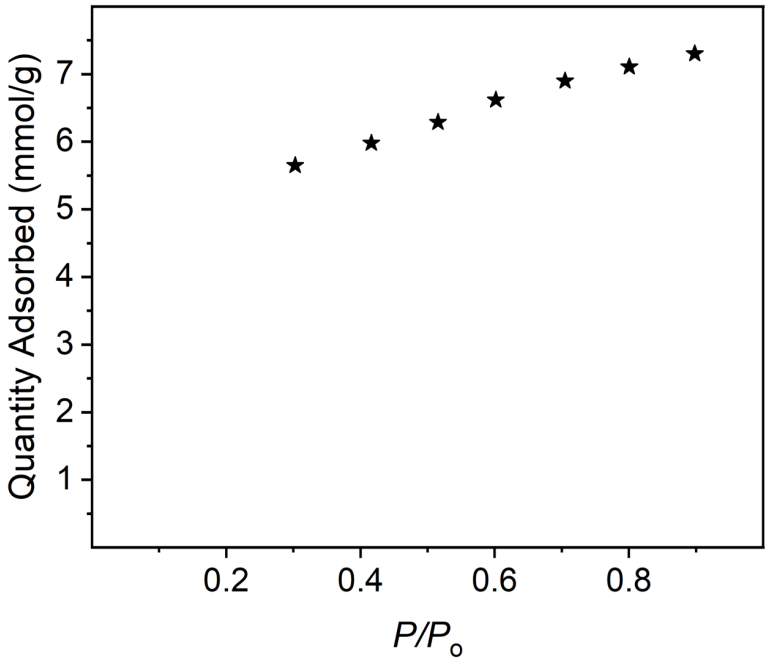

Figure S2.3. Partial N_2 adsorption isotherm measured at 77 K for the (sc4a)Fe(btc) cage, which gives a Langmuir surface area of 850 m^2/g.

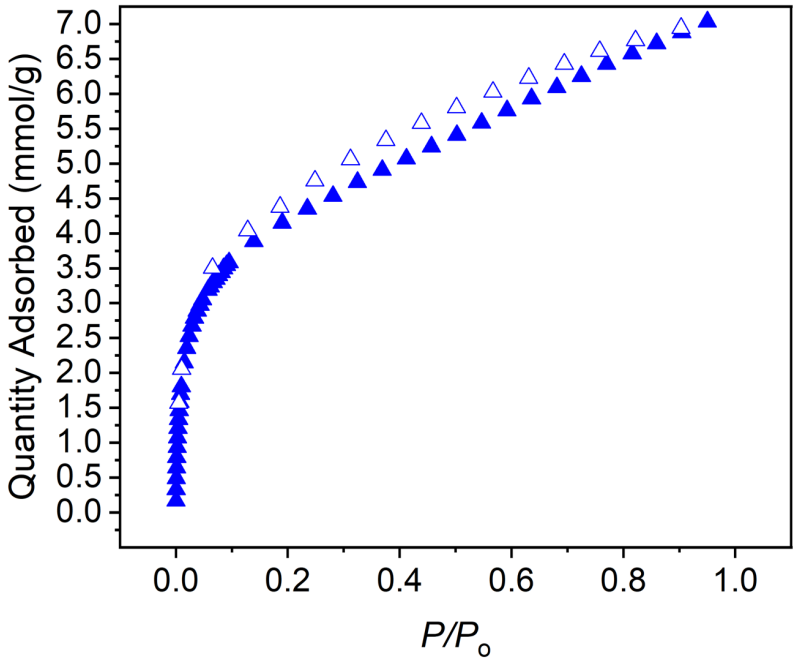

Figure S2.4. CO_2 adsorption (closed triangles) and desorption (open triangles) measured at 195 K for the (sc4a)Fe(bdc) cage.

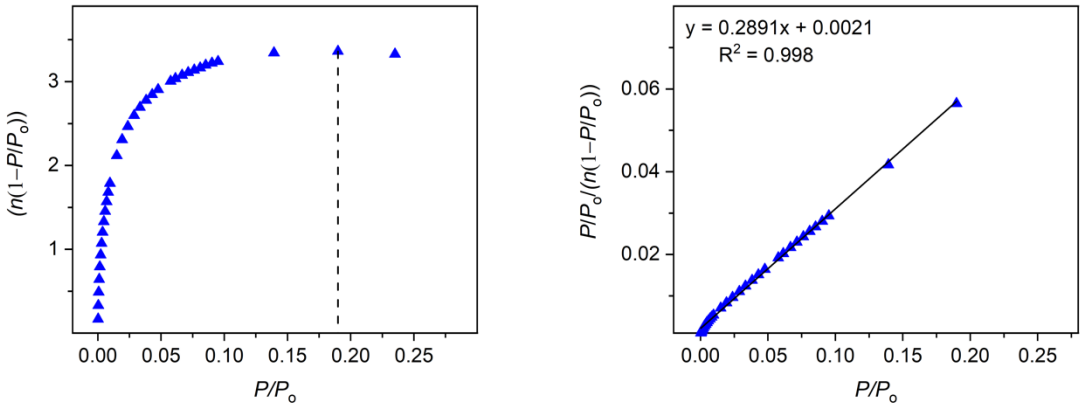

Figure S2.5. Left: Plot of n(1-P/P_0) vs. P/P_0 to determine the maximum P/P_0 used in the BET linear fit according to the first BET consistency criterion for CO_2 adsorption at 195 K for the (sc4a)Fe(bdc) cage. Right: The slope of the best fit line for $P/P_0 < 0.190$ is 0.2891 and the y-intercept is 0.0021, which satisfies the second BET consistency criterion. This results in a measured surface area of 354 m^2/g.

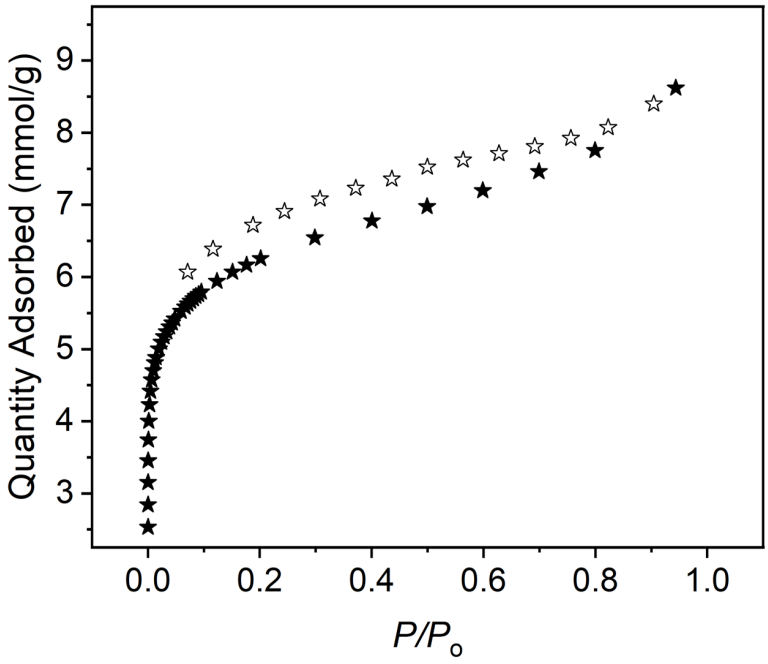

Figure S2.6. N_2 adsorption (closed stars) and desorption (open stars) measured at 77 K for the (sc4a)Fe(bdc) cage.

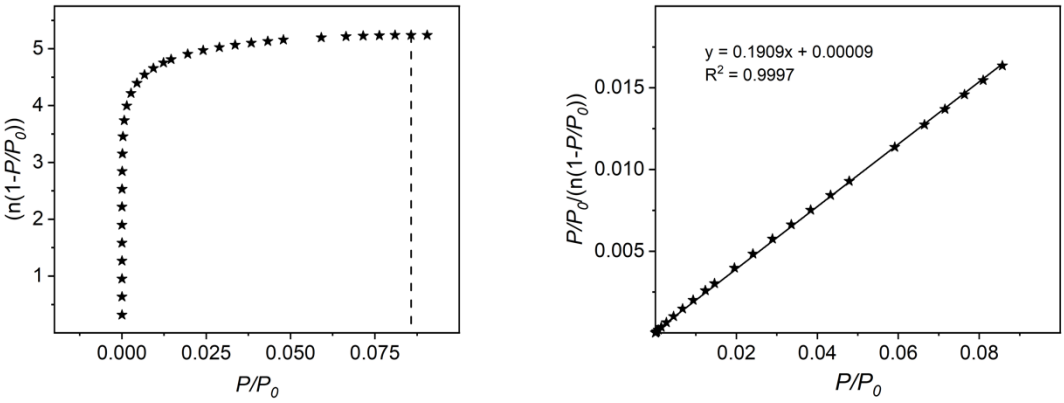

Figure S2.7. Left: Plot of n(1-P/P_0) vs. P/P_0 to determine the maximum P/P_0 used in the BET linear fit according to the first BET consistency criterion for N_2 adsorption at 77 K for the (sc4a)Fe(bdc) cage. Right: The slope of the best fit line for $P/P_0 < 0.086$ is 0.1909 and the y-intercept is 0.00009, which satisfies the second BET consistency criterion. This results in a measured surface area of 511 m^2/g.

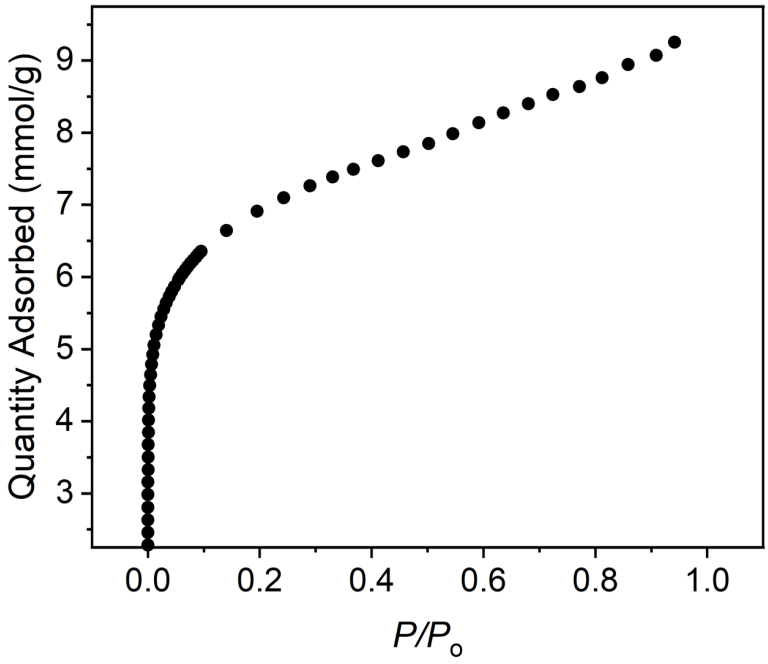

Figure S2.8. Ar adsorption (closed circles) isotherm measured at 77 K for the (sc4a)Fe(bdc) cage.

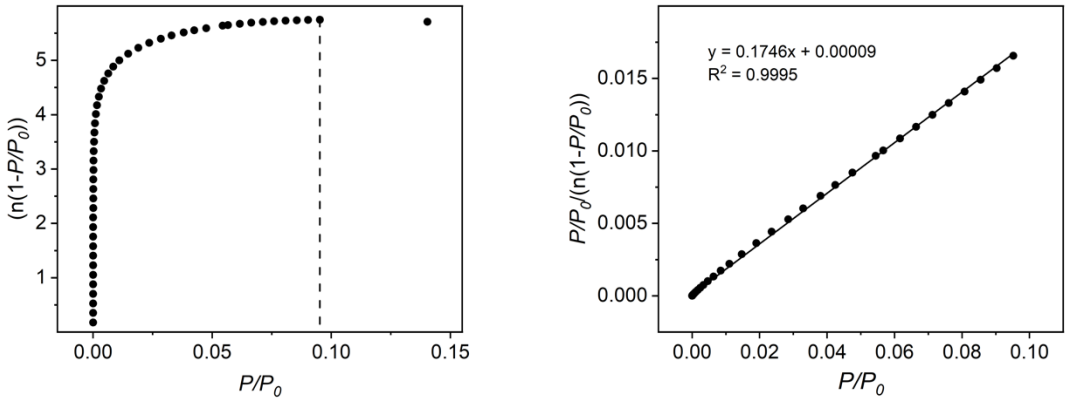

Figure S2.9. Left: Plot of n(1-P/P_0) vs. P/P_0 to determine the maximum P/P_0 used in the BET linear fit according to the first BET consistency criterion for Ar adsorption at 77 K for the (sc4a)Fe(bdc) cage. Right: The slope of the best fit line for $P/P_0 < 0.140$ is 0.1746 and the y-intercept is 0.00009, which satisfies the second BET consistency criterion. This results in a measured surface area of 490 m^2/g.

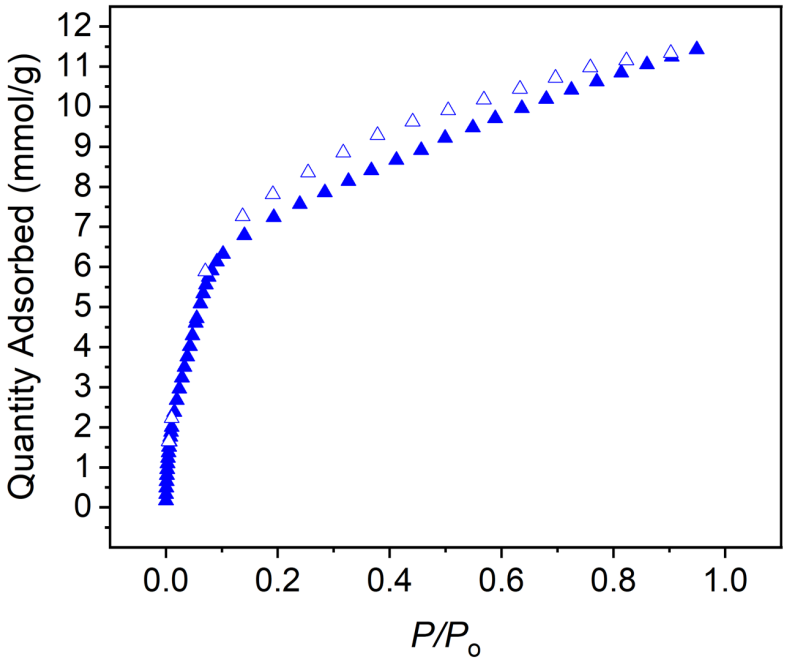

Figure S2.10. CO_2 adsorption (closed triangles) and desorption (open triangles) measured at 195 K for the (sc4a)Fe(tatb) cage.

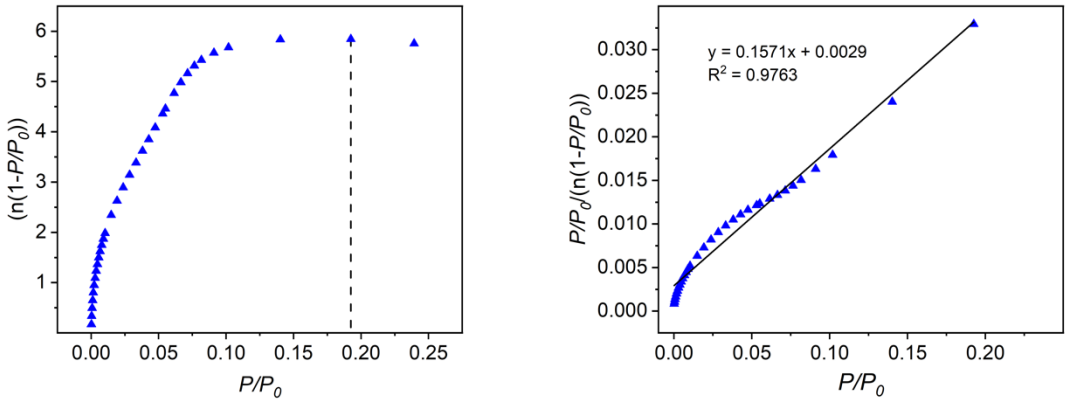

Figure S2.11. Left: Plot of n(1-P/P_0) vs. P/P_0 to determine the maximum P/P_0 used in the BET linear fit according to the first BET consistency criterion for CO_2 adsorption at 195 K for the (sc4a)Fe(tatb) cage. Right: The slope of the best fit line for $P/P_0 < 0.20$ is 0.1571 and the y-intercept is 0.0029, which satisfies the second BET consistency criterion. This results in a measured surface area of 652 m^2/g.

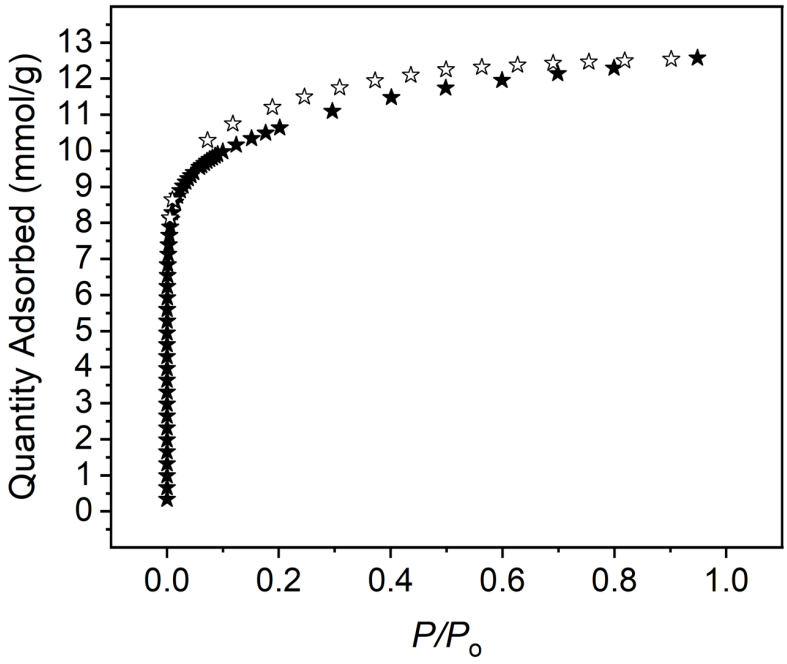

Figure S2.12. N_2 adsorption (closed stars) and desorption (open stars) measured at 77 K for the (sc4a)Fe(tatb) cage.

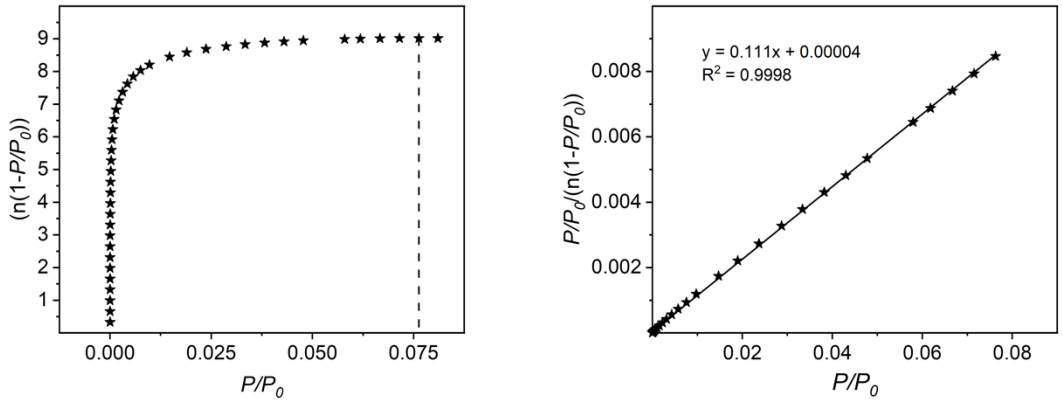

Figure S2.13. Left: Plot of n(1-P/P_0) vs. P/P_0 to determine the maximum P/P_0 used in the BET linear fit according to the first BET consistency criterion for N_2 adsorption at 77 K for the (sc4a)Fe(tatb) cage. Right: The slope of the best fit line for $P/P_0 < 0.080$ is 0.111 and the y-intercept is 0.00004, which satisfies the second BET consistency criterion. This results in a measured surface area of 879 m^2/g.

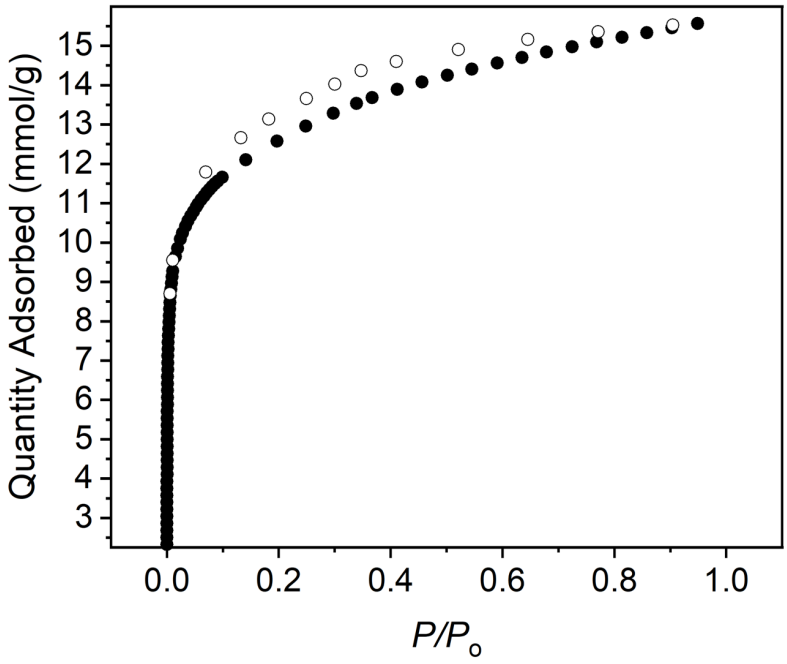

Figure S2.14. Ar adsorption (closed circles) and desorption (open circles) measured at 77 K for the (sc4a)Fe(tatb) cage.

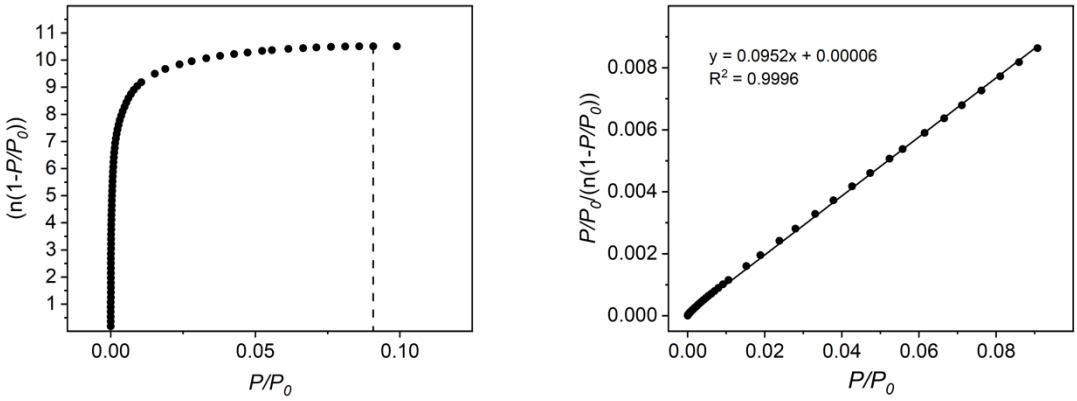

Figure S2.15. Left: Plot of n(1-P/P_0) vs. P/P_0 to determine the maximum P/P_0 used in the BET linear fit according to the first BET consistency criterion for Ar adsorption at 77 K for the (sc4a)Fe(tatb) cage. Right: The slope of the best fit line for $P/P_0 < 0.091$ is 0.0952 and the y-intercept is 0.00006, which satisfies the second BET consistency criterion. This results in a measured surface area of 898 m^2/g.

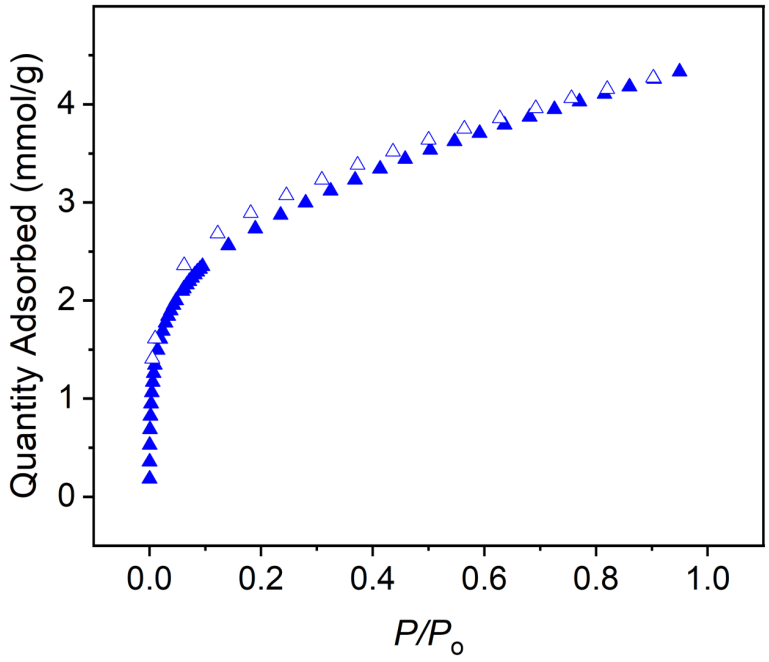

Figure S2.16. CO_2 adsorption (closed triangles) and desorption (open triangles) measured at 195 K for the (tc4a)Fe(btc) cage.

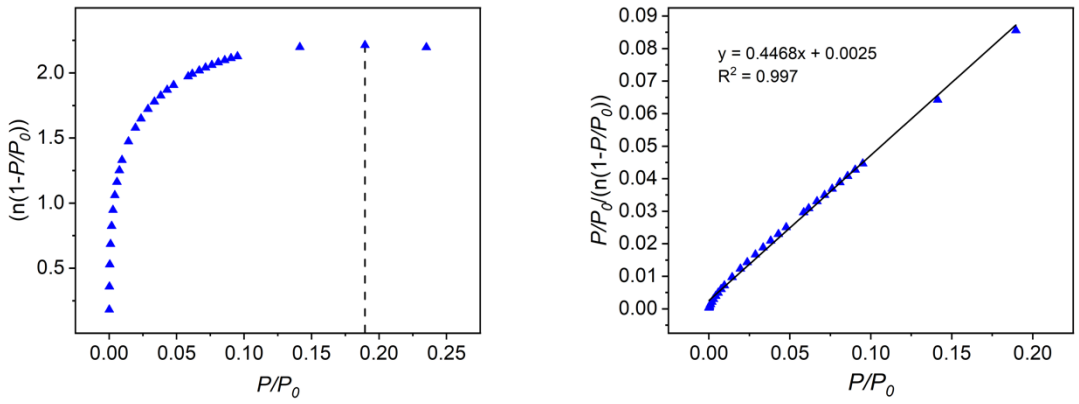

Figure S2.17. Left: Plot of n(1-P/P_0) vs. P/P_0 to determine the maximum P/P_0 used in the BET linear fit according to the first BET consistency criterion for CO_2 adsorption at 195 K for the (tc4a)Fe(btc) cage. Right: The slope of the best fit line for $P/P_0 < 0.20$ is 0.4468 and the y-intercept is 0.0025, which satisfies the second BET consistency criterion. This results in a measured surface area of 229 m^2/g.

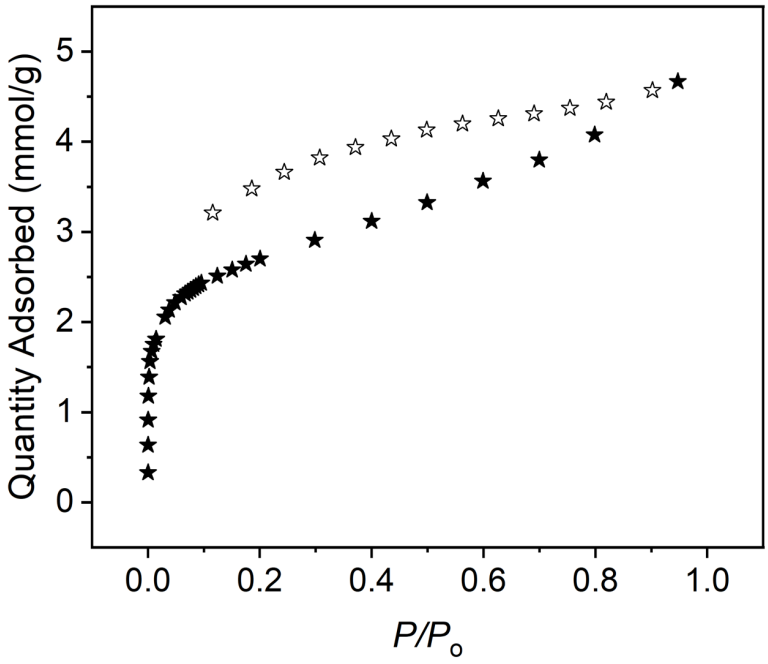

Figure S2.18. N_2 adsorption (closed stars) and desorption (open stars) measured at 77 K for the (tc4a)Fe(btc) cage.

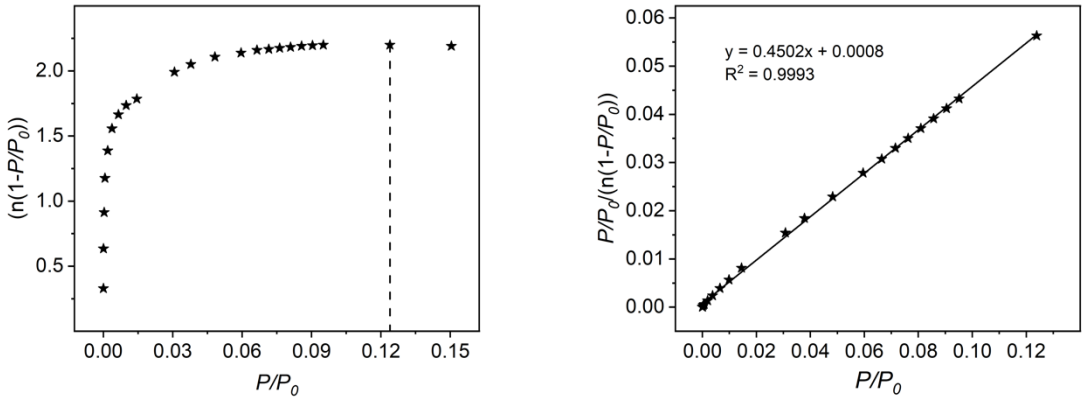

Figure S2.19. Left: Plot of n(1-P/P_0) vs. P/P_0 to determine the maximum P/P_0 used in the BET linear fit according to the first BET consistency criterion for N_2 adsorption at 77 K for the (tc4a)Fe(btc) cage. Right: The slope of the best fit line for $P/P_0 < 0.125$ is 0.4502 and the y-intercept is 0.0008, which satisfies the second BET consistency criterion. This results in a measured surface area of 217 m^2/g.

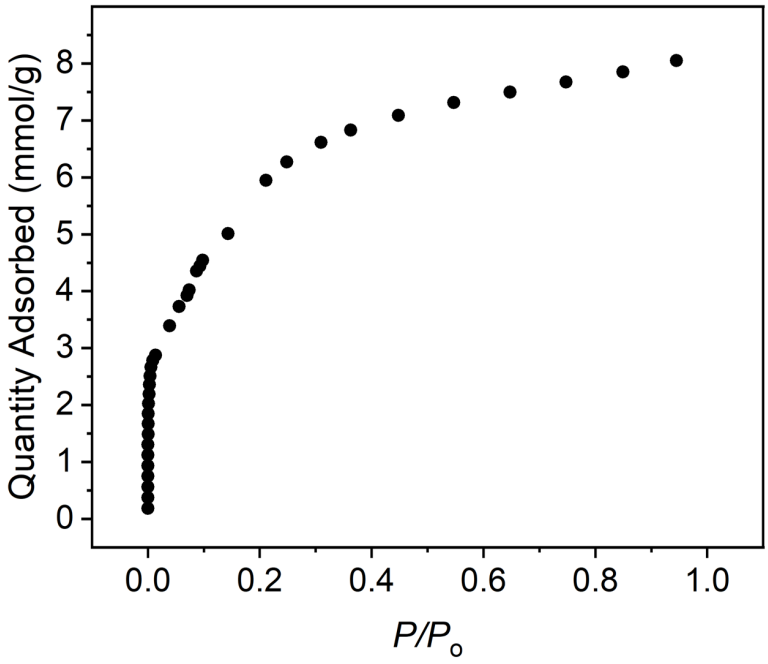

Figure S2.20. Ar adsorption (closed circles) isotherm measured at 77 K for the (tc4a)Fe(btc) cage.

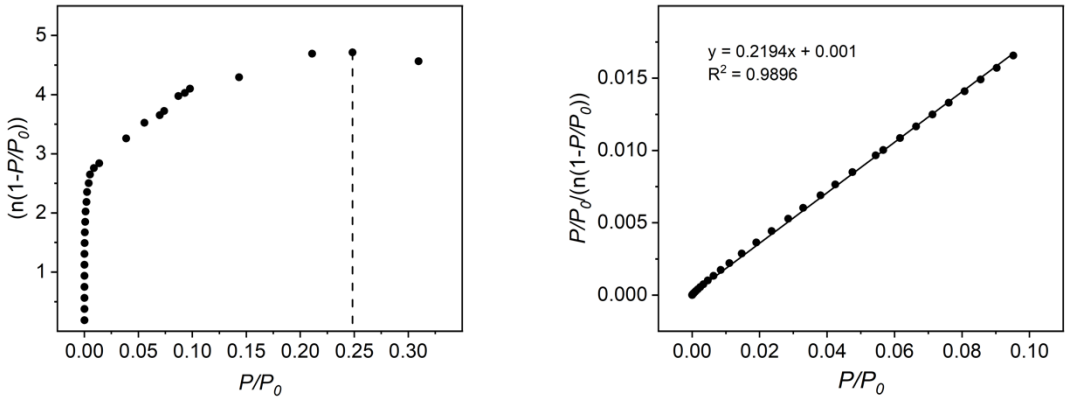

Figure S2.21. Left: Plot of n(1-P/P_0) vs. P/P_0 to determine the maximum P/P_0 used in the BET linear fit according to the first BET consistency criterion for Ar adsorption at 77 K for the (tc4a)Fe(btc) cage. Right: The slope of the best fit line for $P/P_0 < 0.25$ is 0.2194 and the y-intercept is 0.001, which satisfies the second BET consistency criterion. This results in a measured surface area of 390 m^2/g.

Table S2.1. Summary of surface areas measured for the synthesized Fe cages measured at 195 K for CO_2 or 77 K for N_2 and Ar.

	(sc4a)Fe(btc)	(sc4a)Fe(bdc)	(sc4a)Fe(tatb)	(tc4a)Fe(btc)
CO_2 BET	368 m^2/g	354 m^2/g	652 m^2/g	229 m^2/g
CO_2 Langmuir	623 m^2/g	670 m^2/g	1082 m^2/g	408 m^2/g
N_2 BET	--	511 m^2/g	879 m^2/g	217 m^2/g
N_2 Langmuir	850 m^2/g	787 m^2/g	1248 m^2/g	437 m^2/g
Ar BET	--	490 m^2/g	898 m^2/g	390 m^2/g
Ar Langmuir	--	989 m^2/g	1497 m^2/g	802 m^2/g

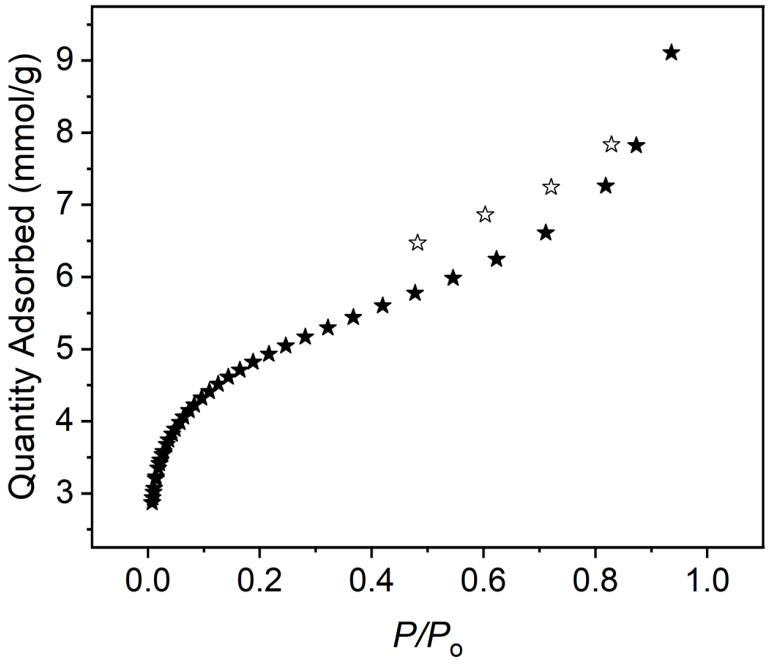

Figure S2.22. N_2 adsorption (closed stars) and desorption (open stars) measured at 77 K for the (sc4a)Fe(btc) cage oxidized with 6 equiv. of magic blue.

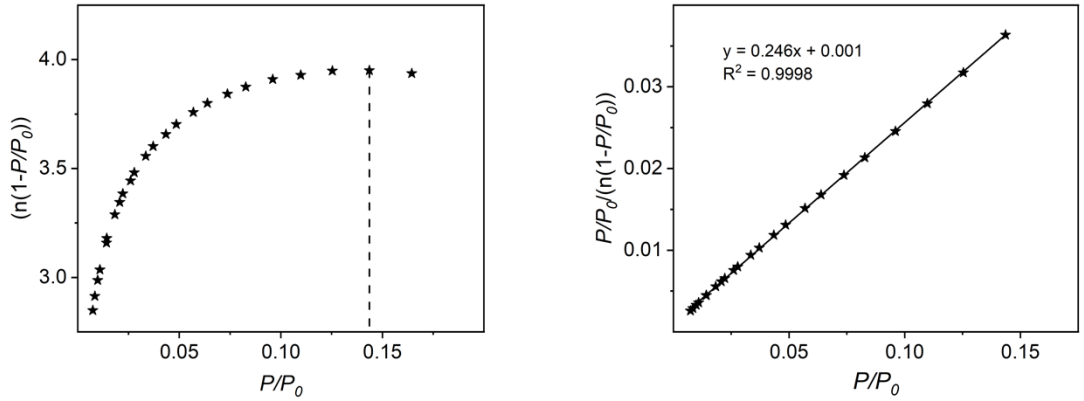

Figure S2.23. Left: Plot of n(1-P/P_0) vs. P/P_0 to determine the maximum P/P_0 used in the BET linear fit according to the first BET consistency criterion for N_2 adsorption at 77 K for the cage generated upon oxidation with 6 equiv. of magic blue. Right: The slope of the best fit line for $P/P_0 < 0.144$ is 0.246 and the y-intercept is 0.001, which satisfies the second BET consistency criterion. This results in a measured surface area of 397 m^2/g.

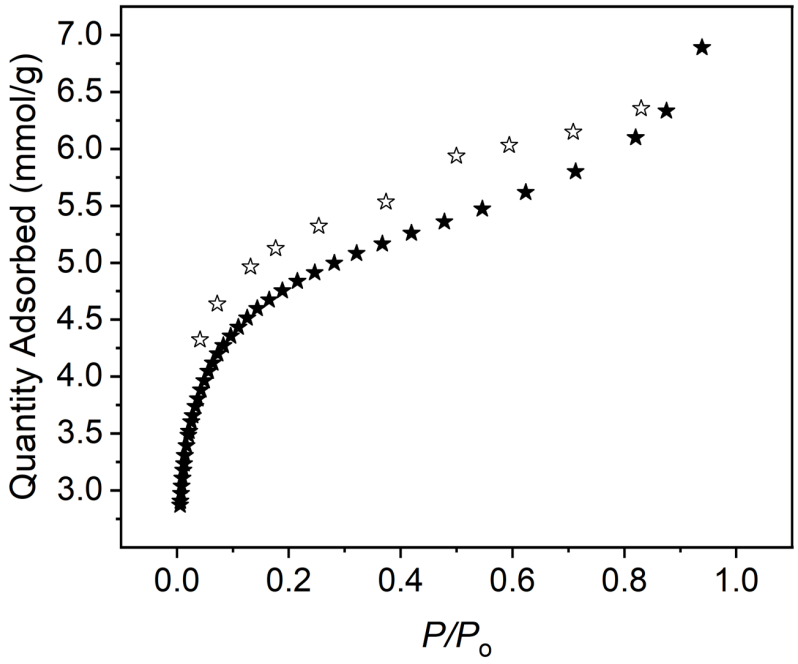

Figure S2.24. N_2 adsorption (closed stars) and desorption (open stars) measured at 77 K for the (sc4a)Fe(btc) cage oxidized with 12 equiv. of magic blue.

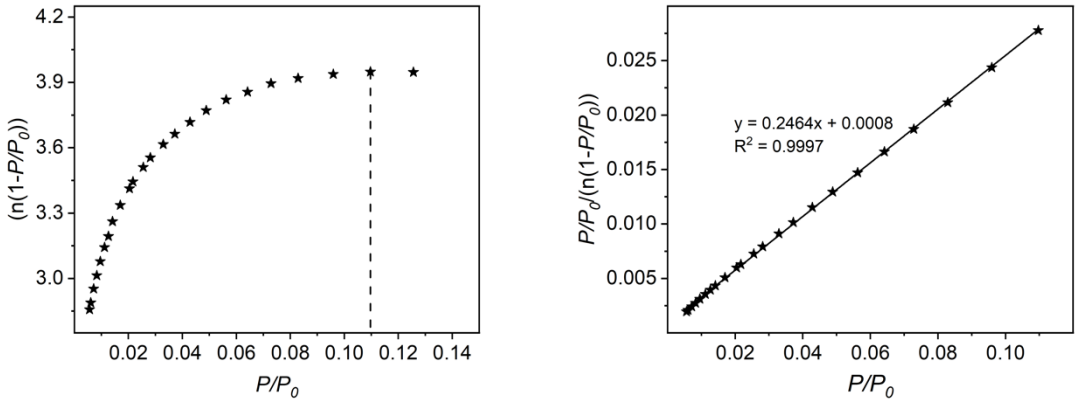

Figure S2.25. Left: Plot of n(1-P/P_0) vs. P/P_0 to determine the maximum P/P_0 used in the BET linear fit according to the first BET consistency criterion for N_2 adsorption at 77 K for the cage generated upon oxidation with 12 equiv. of magic blue. Right: The slope of the best fit line for $P/P_0 < 0.110$ is 0.2464 and the y-intercept is 0.0008, which satisfies the second BET consistency criterion. This results in a measured surface area of 396 m^2/g.

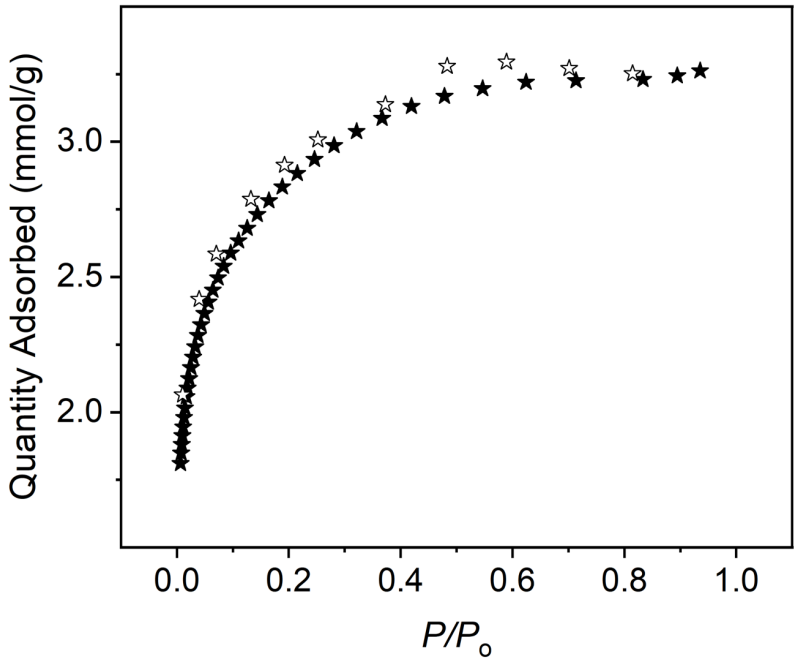

Figure S2.26. N_2 adsorption (closed stars) and desorption (open stars) measured at 77 K for the (sc4a)Fe(btc) cage oxidized with 18 equiv. of magic blue.

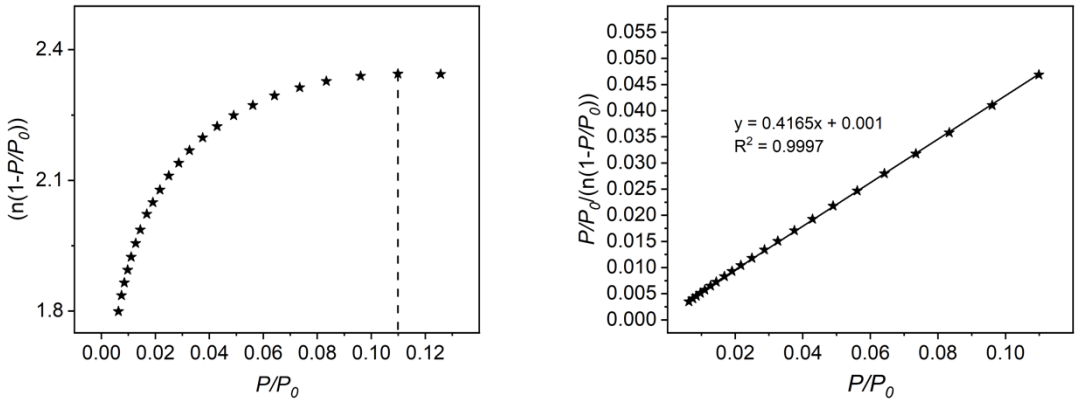

Figure S2.27. Left: Plot of n(1-P/P_0) vs. P/P_0 to determine the maximum P/P_0 used in the BET linear fit according to the first BET consistency criterion for N_2 adsorption at 77 K for the cage generated upon oxidation with 18 equiv. of magic blue. Right: The slope of the best fit line for $P/P_0 < 0.110$ is 0.4165 and the y-intercept is 0.0012, which satisfies the second BET consistency criterion. This results in a measured surface area of 234 m^2/g.

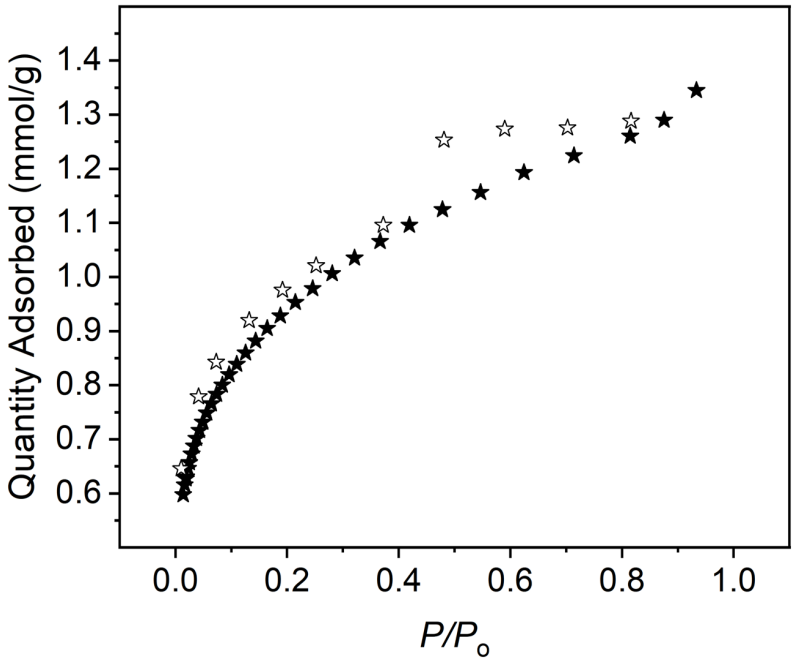

Figure S2.28. N_2 adsorption (closed stars) and desorption (open stars) measured at 77 K for the (sc4a)Fe(btc) cage oxidized with 24 equiv. of magic blue.

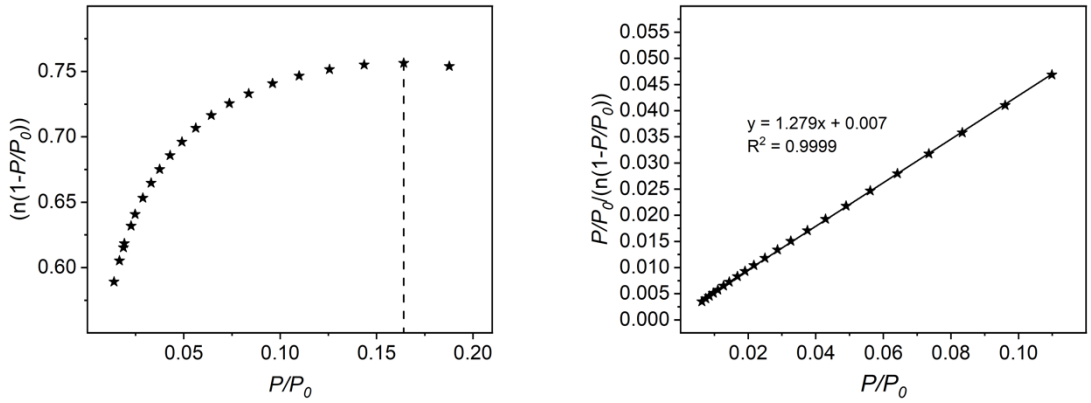

Figure S2.29. Left: Plot of n(1-P/P_0) vs. P/P_0 to determine the maximum P/P_0 used in the BET linear fit according to the first BET consistency criterion for N_2 adsorption at 77 K for the cage generated upon oxidation with 24 equiv. of magic blue. Right: The slope of the best fit line for $P/P_0 < 0.164$ is 1.279 and the y-intercept is 0.007, which satisfies the second BET consistency criterion. This results in a measured surface area of 76 m^2/g.

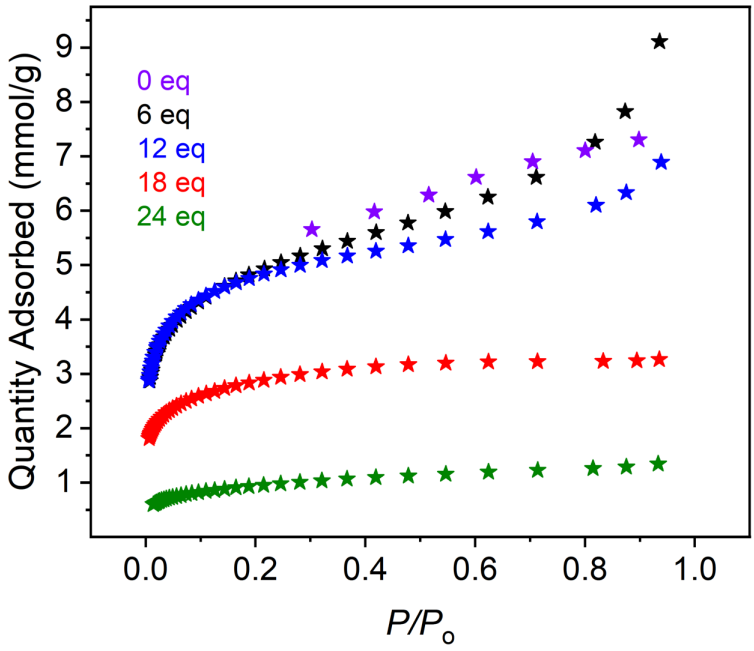

Figure S2.30. Overlay of N_2 adsorption isotherms for the (sc4a)Fe(btc) cage (purple) and the oxidized cages generated upon treatment with 6-24 equiv. of magic blue.

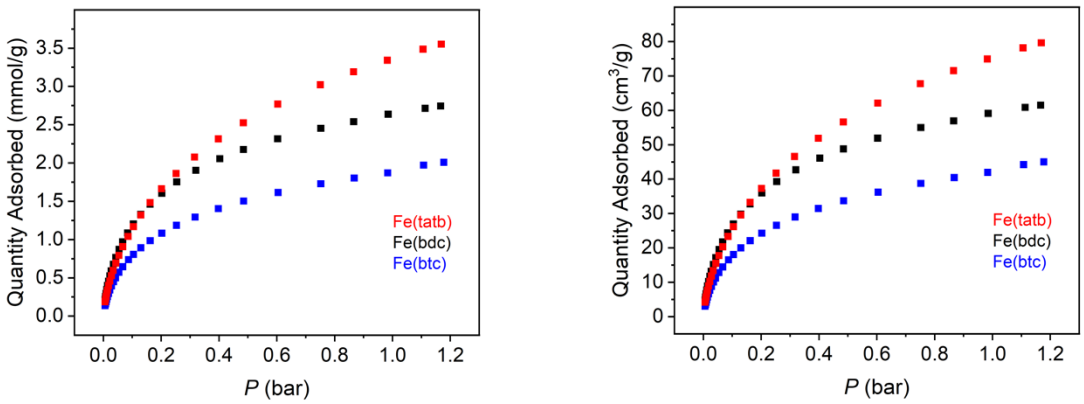

Figure S2.31. Low pressure methane adsorption isotherms measured at 195 K for the (sc4a)Fe(tatb), (sc4a)Fe(bdc) (black), and (sc4a)Fe(btc) (blue) cages. The reported volumetric uptakes are based on measured tap densities for the three cages.

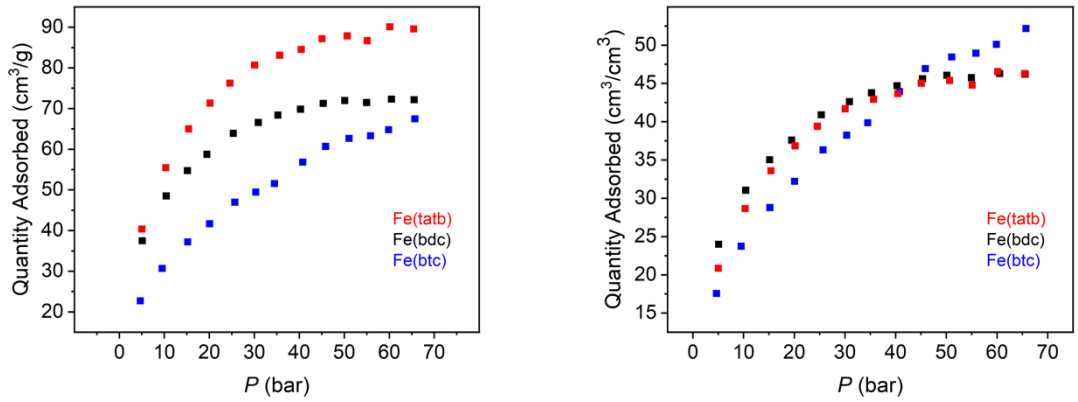

Figure S2.32. High pressure total gravimetric (left) and volumetric (right) methane adsorption isotherms measured at 298 K for the (sc4a)Fe(tatb), (sc4a)Fe(bdc) (black), and (sc4a)Fe(btc) (blue) cages. The reported volumetric uptakes are based on measured tap densities for the three cages.

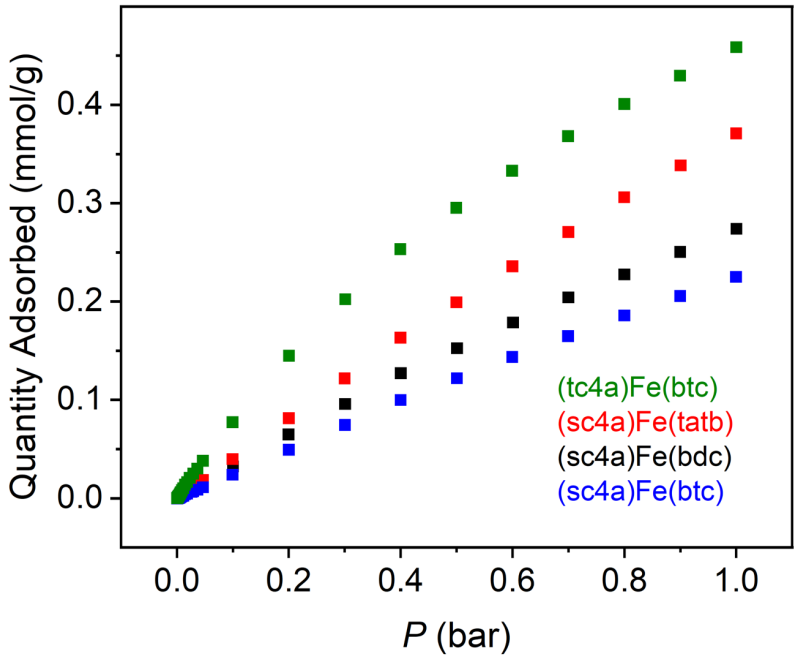

Figure S2.33. Methane adsorption isotherms measured at 298 K for the (tc4a)Fe(btc) (green), (sc4a)Fe(tatb), (sc4a)Fe(bdc) (black), and (sc4a)Fe(btc) (blue) cages.

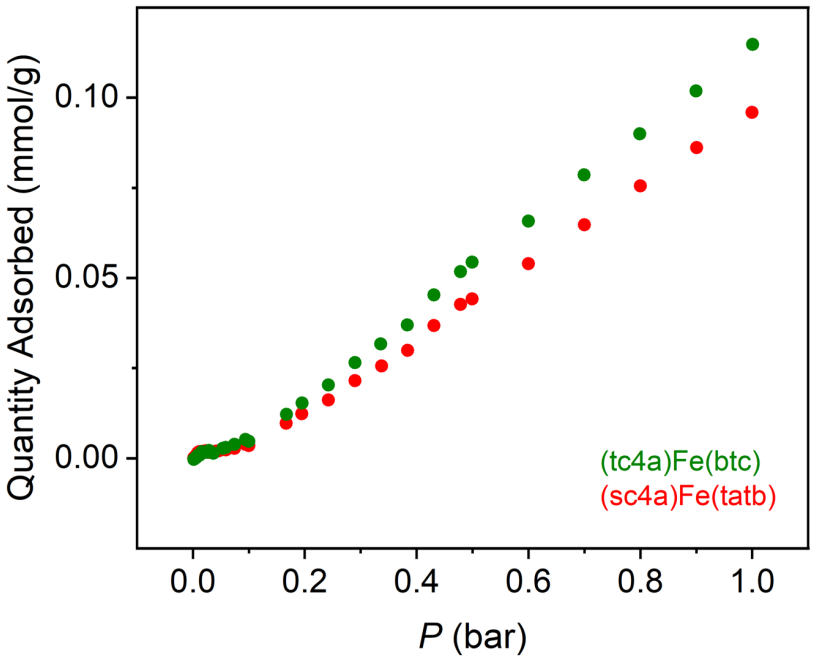

Figure S2.34. Argon adsorption isotherms measured at 298 K for the (tc4a)Fe(btc) (green) and (sc4a)Fe(tatb) (red) cages.

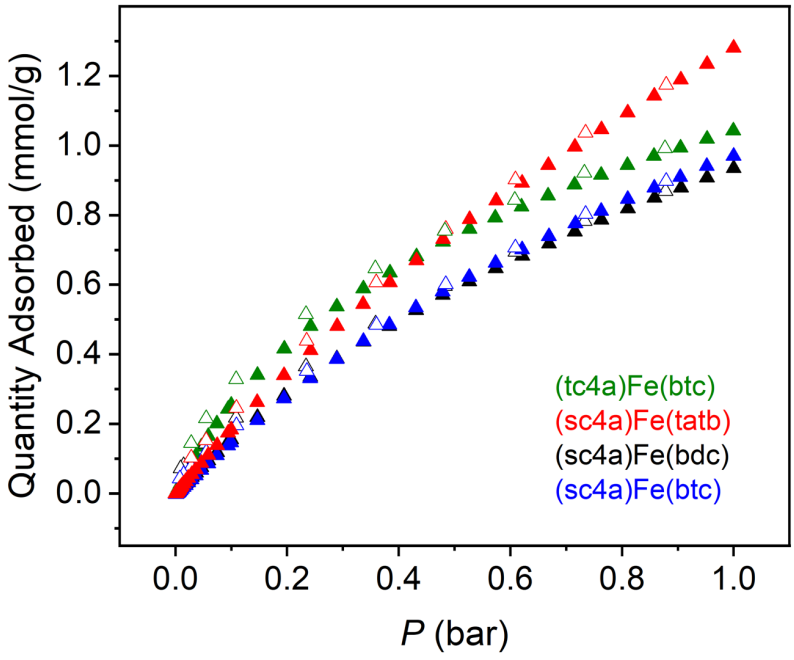

Figure S2.35. CO_2 adsorption and desorption isotherms measured at 298 K for the (tc4a)Fe(btc) (green), (sc4a)Fe(tatb), (sc4a)Fe(bdc) (black), and (sc4a)Fe(btc) (blue) cages.

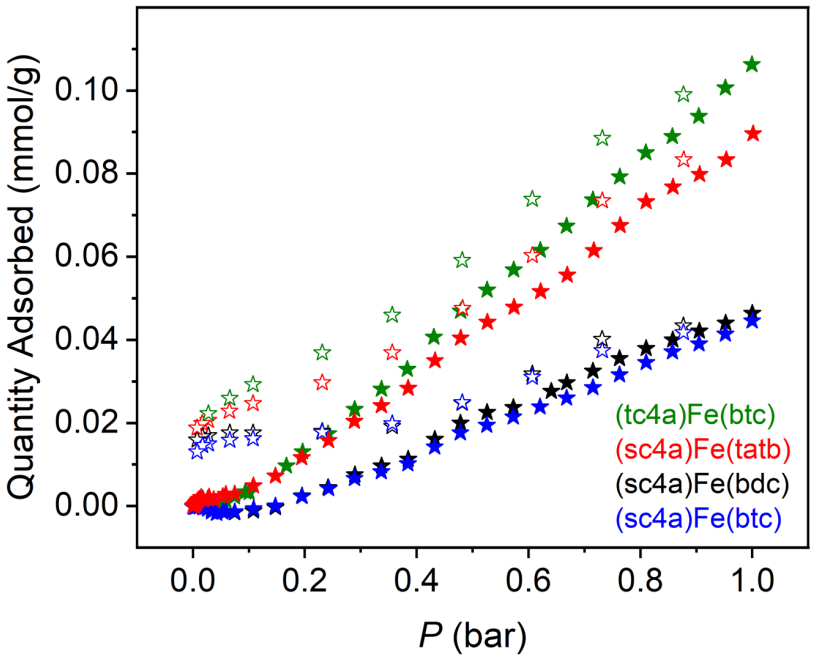

Figure S2.36. N_2 adsorption and desorption isotherms measured at 298 K for the (tc4a)Fe(btc) (green), (sc4a)Fe(tatb), (sc4a)Fe(bdc) (black), and (sc4a)Fe(btc) (blue) cages.

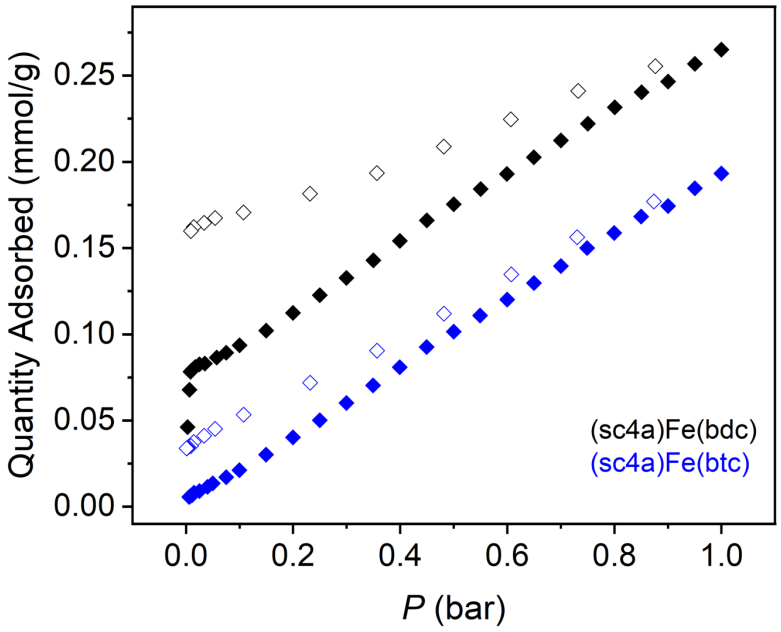

Figure S2.37. O_2 adsorption and desorption isotherms measured at 273 K for the (sc4a)Fe(bdc) (black) and (sc4a)Fe(btc) (blue) cages.

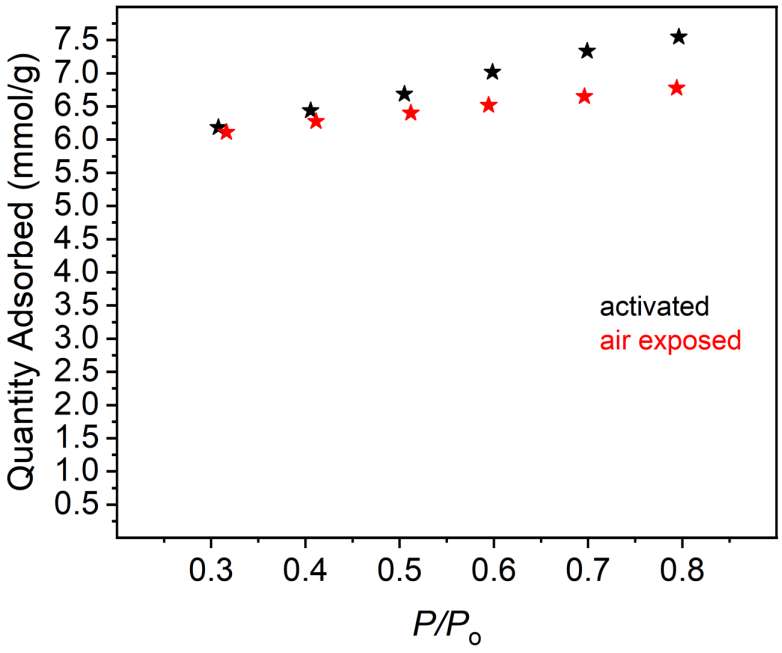

Figure S2.38. N_2 adsorption isotherms measured at 77 K for the (sc4a)Fe(btc) cage obtained for material activated under optimized conditions (black) and following exposure to air overnight and reactivation (red). The plotted data represent two separate batches of material.

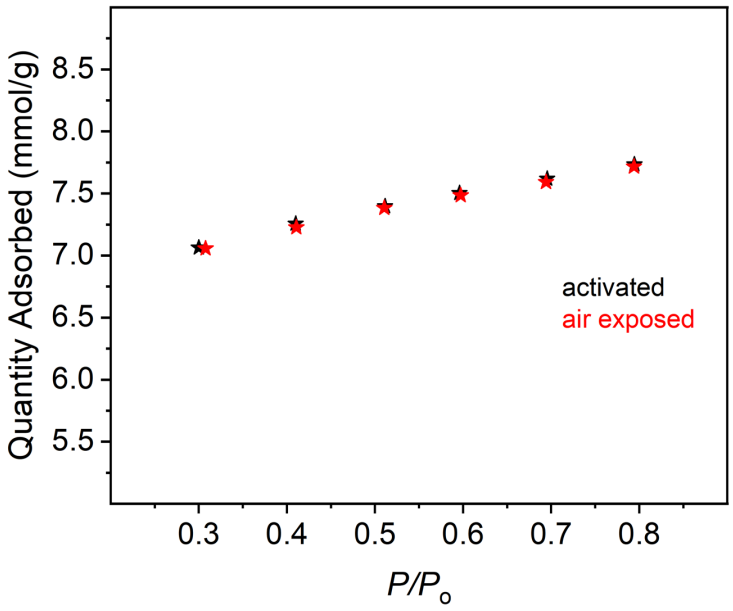

Figure S2.39. N_2 adsorption isotherms measured at 77 K for the (sc4a)Fe(bdc) cage obtained for material activated under optimized conditions (black) and following exposure to air overnight and reactivation (red). The plotted data are for the same sample.

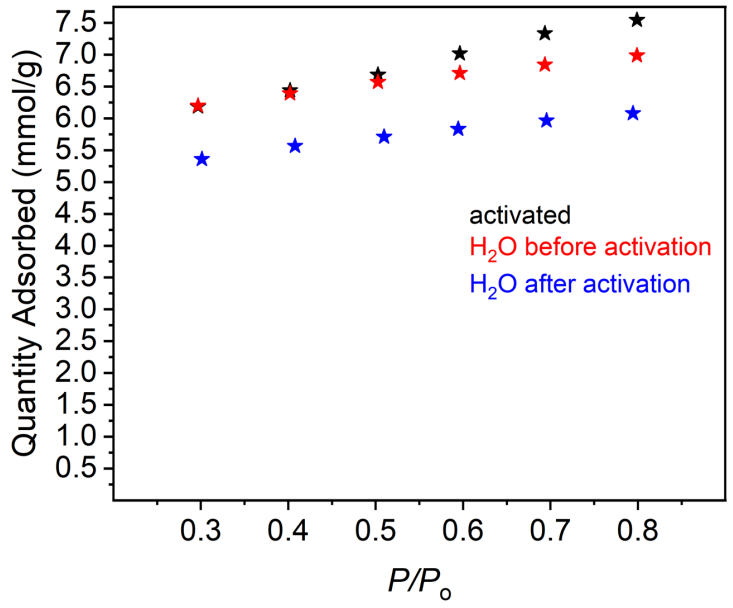

Figure S2.40. N_2 adsorption isotherms measured at 77 K for the (sc4a)Fe(btc) cage obtained for material activated under optimized conditions (black) and following exposure of the same sample to water overnight and reactivation (blue). Exposure of the Et_2O exchanged material to water overnight followed by vacuum activation is plotted in red.

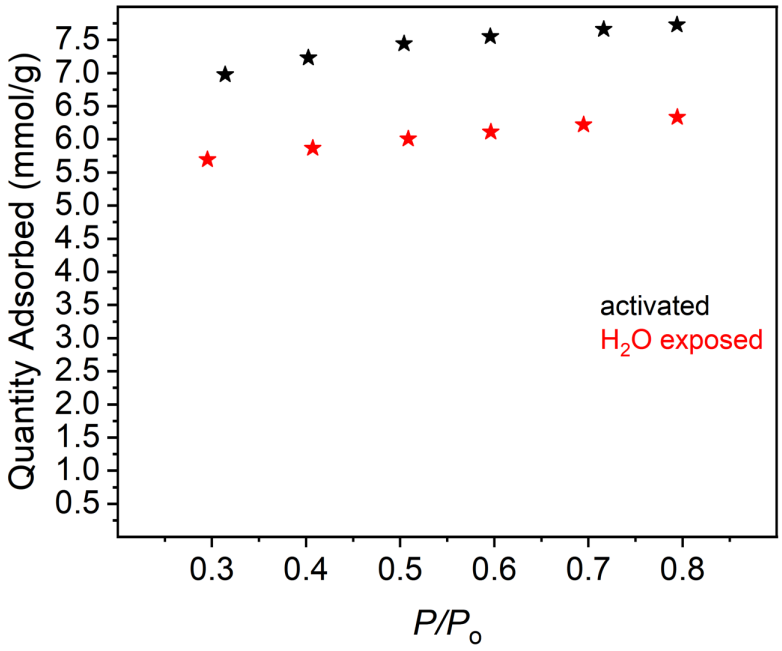

Figure S2.41. N_2 adsorption isotherms measured at 77 K for the (sc4a)Fe(bdc) cage obtained for material activated under optimized conditions (black) and following exposure of the same sample to water overnight and reactivation (red).

Fitting of Isotherms

The adsorption isotherms were fit with single-, dual-, or triple-site Langmuir-Freundlich model (Eqn. 1), where n is the absolute amount adsorbed in mmol/g, P is the pressure in bar, $q_{sat,i}$ is the saturation capacity in mmol/g, b_i is the Langmuir parameter in bar^{-1}, and v_i is the Freundlich parameter for site 1. The parameters used to fit the adsorption isotherms can be found in Tables S2.2-S2.13. Plots of the adsorption isotherms along with their fits are presented in Figures S2.42-S2.53.

Equation 1. $$n = \frac{q_{sat,1} b_1 P^{v_1}}{1+b_1 P^{v_1}} + \frac{q_{sat,2} b_2 P^{v_2}}{1+b_2 P^{v_2}} + \frac{q_{sat,3} b_3 P^{v_3}}{1+b_3 P^{v_3}}$$

The isosteric heats of adsorption, -Q_{st}, were calculated through the use of the Clausius-Clapyron equation (Eqn 2) for each gas using single-site Langmuir-Freundlich fits for each material at either 288 K, 298 K, and 308 K (ethylene, ethane, and propylene) or 273 K, 288 K, and 298 K (propane). P is the pressure, n is the amount adsorbed, T is the temperature, R is the universal gas constant, and C is a constant. Based on plots of $(\ln P)_n$ as a function of $1/T$ the isosteric heat adsorption was obtained by the slope.

Equation 2. $$ln\, P = -\frac{Q_{st}}{R}\left(\frac{1}{T}\right) + C$$

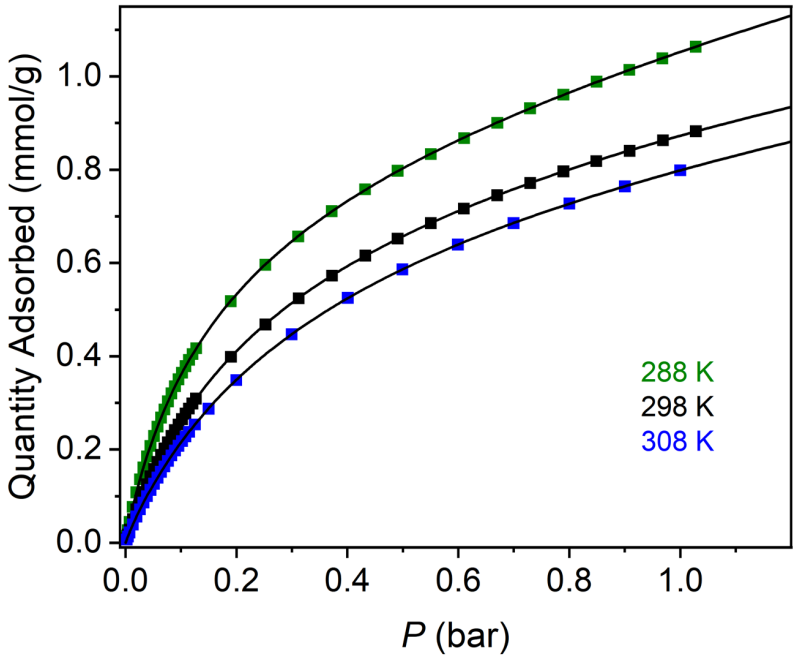

Figure S2.42. Pure component isotherm data for ethane adsorption in (sc4a)Fe(btc). Experimental data are plotted as closed squares for isotherms measured at 288 K (green), 298 K (black), and 308 K (blue). The black lines are the respective dual-site Langmuir-Freundlich fits using the parameters in Table S2.2.

Table S2.2.

	288 K	**298 K**	**308 K**
$q_{sat,1}$ (mmol/g)	0.850600	0.508630	0.99415
b_1 (bar)	5.112010	5.308920	2.25561
v_1	0.930380	1.053670	0.92866
$q_{sat,2}$ (mmol/g)	6.279120	2.358230	45.30145
b_2 (bar)	0.057450	0.232490	0.00243
v_2	0.933300	0.720420	1.20778

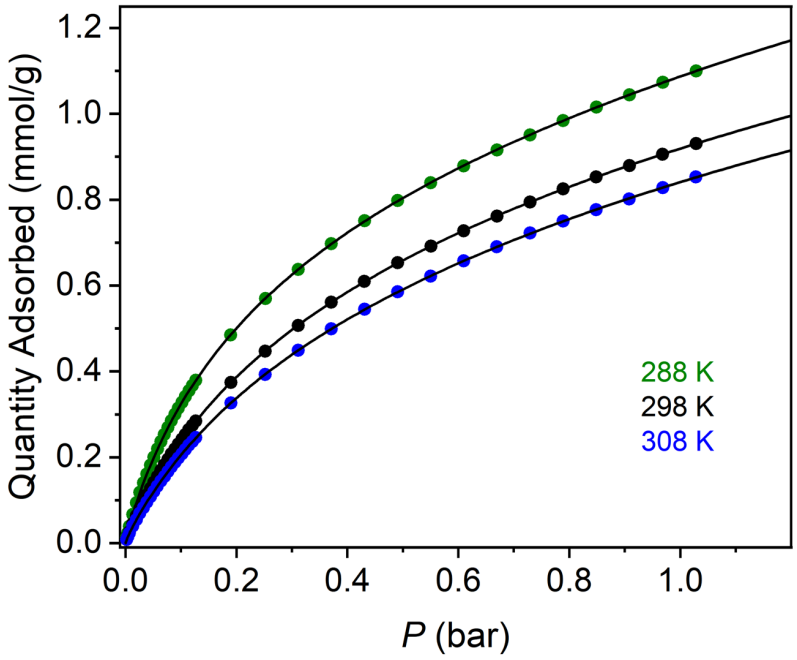

Figure S2.43. Pure component isotherm data for ethylene adsorption in (sc4a)Fe(btc). Experimental data are plotted as closed circles for isotherms measured at 288 K (green), 298 K (black), and 308 K (blue). The black lines are the respective dual-site Langmuir-Freundlich fits using the parameters in Table S2.3.

Table S2.3.

	288 K	**298 K**	**308 K**
$q_{sat,1}$ (mmol/g)	0.92912	0.480080	0.314050
b_1 (bar)	3.28625	3.840760	4.243390
v_1	0.89557	1.013640	1.087510
$q_{sat,2}$ (mmol/g)	2.93392	2.624640	2.502620
b_2 (bar)	0.14641	0.257910	0.306310
v_2	0.92109	0.774250	0.766660

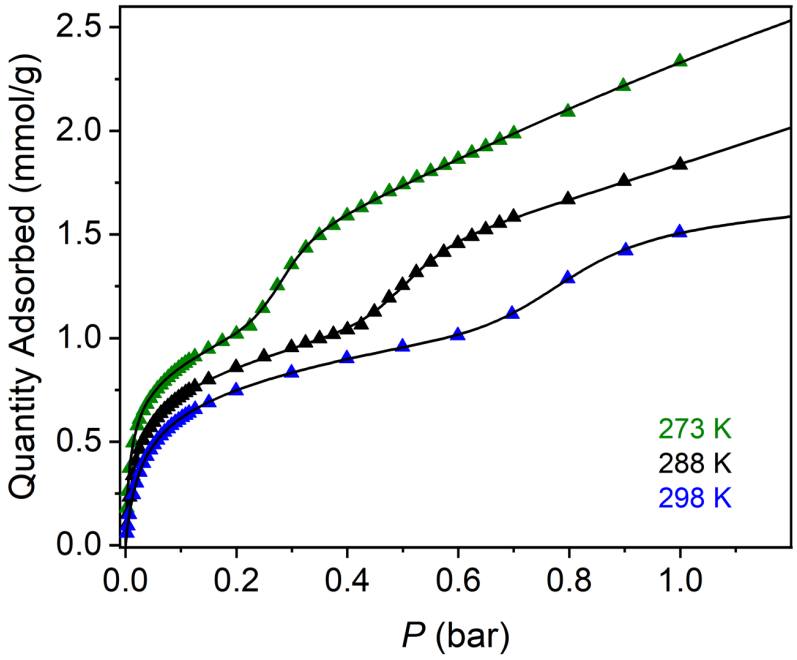

Figure S2.44. Pure component isotherm data for propane adsorption in (sc4a)Fe(btc). Experimental data are plotted as closed triangles for isotherms measured at 273 K (green), 288 K (black), and 298 K (blue). The black lines are the respective three-site Langmuir-Freundlich fits using the parameters in Table S2.4.

Table S2.4.

	273 K	**288 K**	**298 K**
$q_{sat,1}$ (mmol/g)	0.31972	99.99999	2.97076
b_1 (bar)	267530.8857	0.00685	0.2768
v_1	9.95711	1.23845	0.59074
$q_{sat,2}$ (mmol/g)	0.94897	0.89061	0.51266
b_2 (bar)	31.921	23.05768	47.96543
v_2	0.79369	0.84379	1.04072
$q_{sat,3}$ (mmol/g)	3.66087	0.30592	0.38669
b_3 (bar)	0.42375	2947.62452	13.63178
v_3	1.36598	11.87613	11.02253

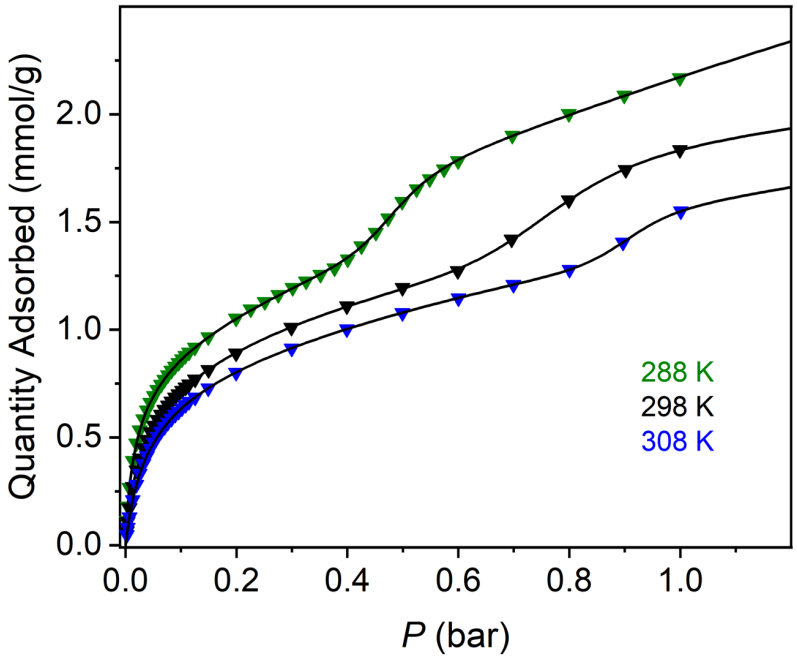

Figure S2.45. Pure component isotherm data for propylene adsorption in (sc4a)Fe(btc). Experimental data are plotted as inverted triangles for isotherms measured at 288 K (green), 298 K (black), and 308 K (blue). The black lines are the respective three-site Langmuir-Freundlich fits using the parameters in Table S2.5.

Table S2.5.

	288 K	**298 K**	**308 K**
$q_{sat,1}$ (mmol/g)	0.28839	2.36312	3.30743
b_1 (bar)	7334.68481	0.60789	0.26527
v_1	12.2701	0.72111	0.82598
$q_{sat,2}$ (mmol/g)	0.86302	0.57187	0.70296
b_2 (bar)	30.26509	47.19507	23.69923
v_2	0.8695	1.0136	0.96109
$q_{sat,3}$ (mmol/g)	49.99998	0.40988	0.20351
b_3 (bar)	0.02143	12.50853	8.00821
v_3	0.80782	9.80858	21.33938

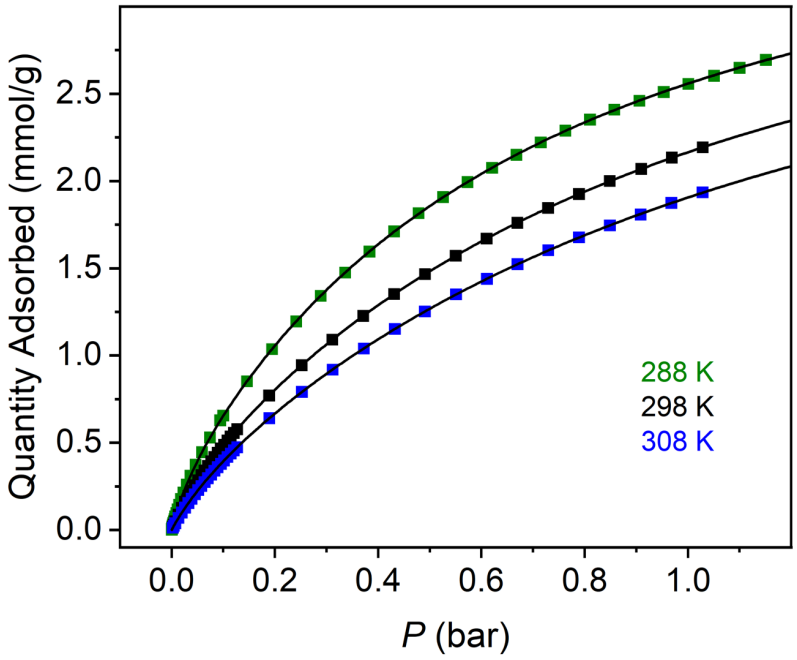

Figure S2.46. Pure component isotherm data for ethane adsorption in (sc4a)Fe(tatb). Experimental data are plotted as closed squares for isotherms measured at 288 K (green), 298 K (black), and 308 K (blue). The black lines are the respective dual-site Langmuir-Freundlich fits using the parameters in Table S2.6.

Table S2.6.

	288 K	**298 K**	**308 K**
$q_{sat,1}$ (mmol/g)	3.49834	2.862230	3.165880
b_1 (bar)	1.52685	1.050800	0.840290
v_1	1.1337	1.275370	1.172830
$q_{sat,2}$ (mmol/g)	0.47246	0.817420	0.533900
b_2 (bar)	15.82495	5.860340	6.222550
v_2	0.95194	0.931780	0.932350

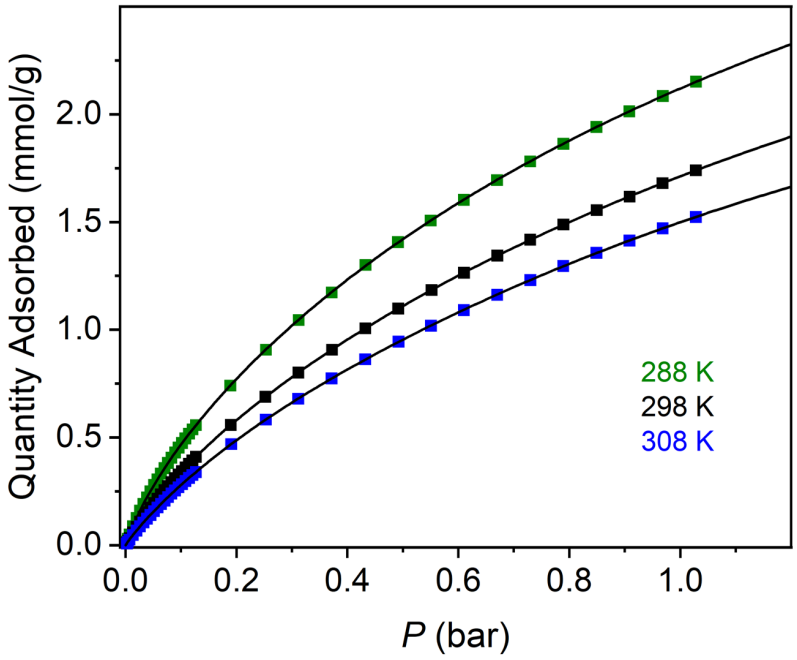

Figure S2.47. Pure component isotherm data for ethylene adsorption in (sc4a)Fe(tatb). Experimental data are plotted as closed circles for isotherms measured at 288 K (green), 298 K (black), and 308 K (blue). The black lines are the respective dual-site Langmuir-Freundlich fits using the parameters in Table S2.7.

Table S2.7.

	288 K	**298 K**	**308 K**
$q_{sat,1}$ (mmol/g)	4.88632	4.13411	0.70514
b_1 (bar)	0.6258	0.48641	0.55445
v_1	0.94498	1.01877	2.12096
$q_{sat,2}$ (mmol/g)	0.25857	0.43847	2.38218
b_2 (bar)	11.97392	4.54512	1.09942
v_2	0.97766	0.91181	0.9221

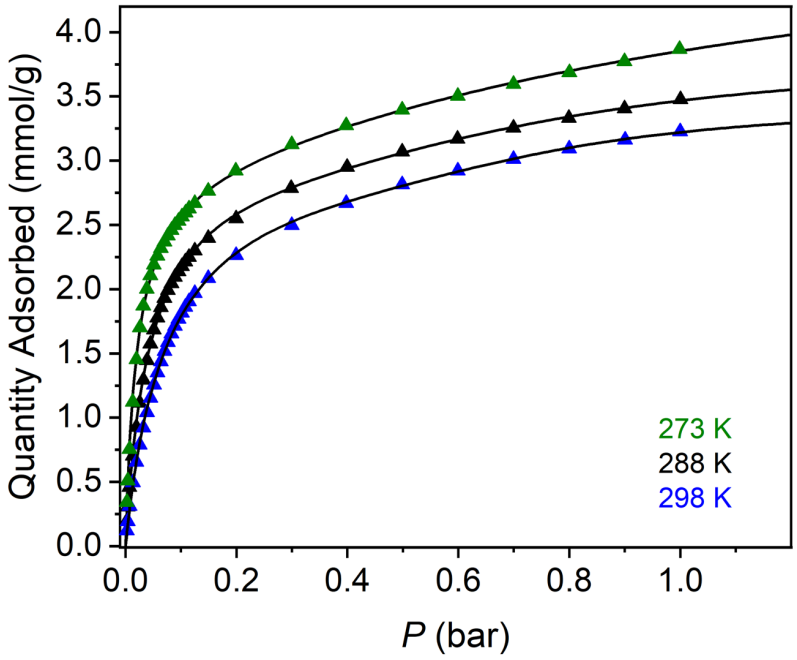

Figure S2.48. Pure component isotherm data for propane adsorption in (sc4a)Fe(tatb). Experimental data are plotted as closed triangles for isotherms measured at 273 K (green), 288 K (black), and 298 K (blue). The black lines are the respective dual-site Langmuir-Freundlich fits using the parameters in Table S2.8.

Table S2.8.

	273 K	**288 K**	**298 K**
$q_{sat,1}$ (mmol/g)	2.996860	3.182660	3.198420
b_1 (bar)	47.364340	19.551970	11.878450
v_1	0.991410	0.965470	0.971020
$q_{sat,2}$ (mmol/g)	2.045280	0.658400	0.344670
b_2 (bar)	0.814450	2.000140	3.670960
v_2	1.262200	2.544550	4.129280

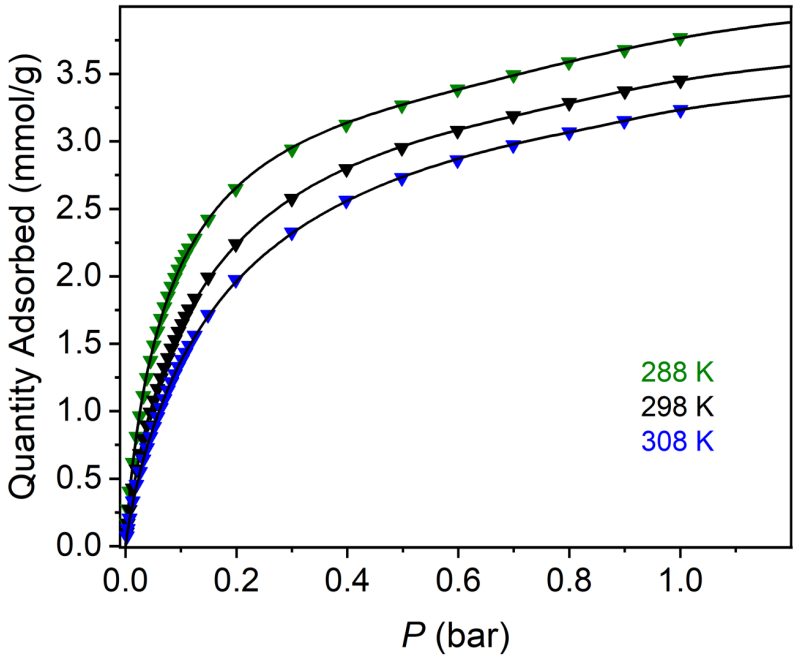

Figure S2.49. Pure component isotherm data for propylene adsorption in (sc4a)Fe(tatb). Experimental data are plotted as inverted triangles for isotherms measured at 288 K (green), 298 K (black), and 308 K (blue). The black lines are the respective dual-site Langmuir-Freundlich fits using the parameters in Table S2.9.

Table S2.9.

	288 K	**298 K**	**308 K**
$q_{sat,1}$ (mmol/g)	3.97903	4.01116	3.99952
b_1 (bar)	8.30976	5.21843	4.00349
v_1	0.87975	0.88315	0.88464
$q_{sat,2}$ (mmol/g)	0.33588	0.11667	0.04019
b_2 (bar)	1.76857	2.81898	5.6009
v_2	5.18714	9.0955	21.56109

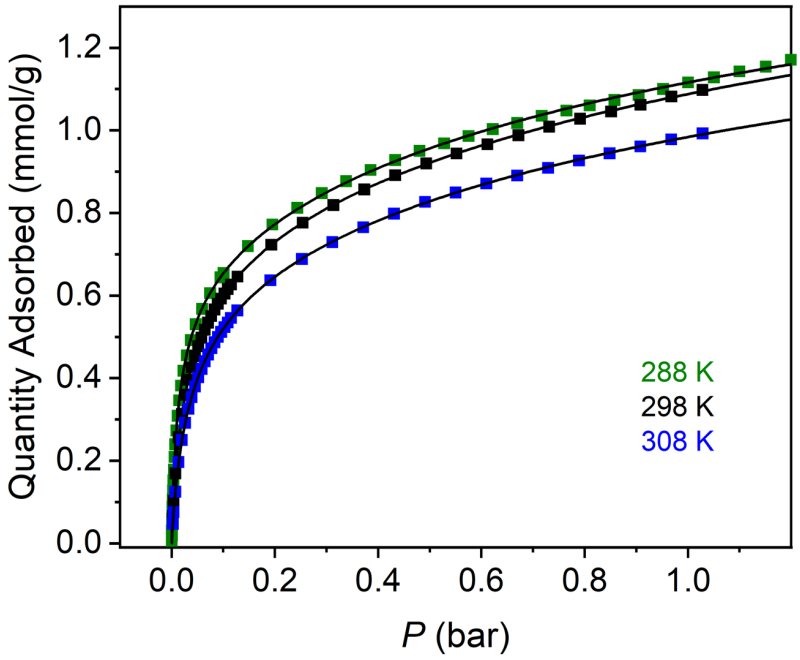

Figure S2.50. Pure component isotherm data for ethane adsorption in (tc4a)Fe(btc). Experimental data are plotted as closed squares for isotherms measured at 288 K (green), 298 K (black), and 308 K (blue). The black lines are the respective dual-site Langmuir-Freundlich fits using the parameters in Table S2.10.

Table S2.10.

	288 K	**298 K**	**308 K**
$q_{sat,1}$ (mmol/g)	1.4868	1.503580	1.2352
b_1 (bar)	0.72768	0.592900	0.67791
v_1	0.64224	0.674970	0.72713
$q_{sat,2}$ (mmol/g)	0.49655	0.544610	0.50274
b_2 (bar)	73.28872	32.150840	27.15573
v_2	0.9556	0.921770	0.94179

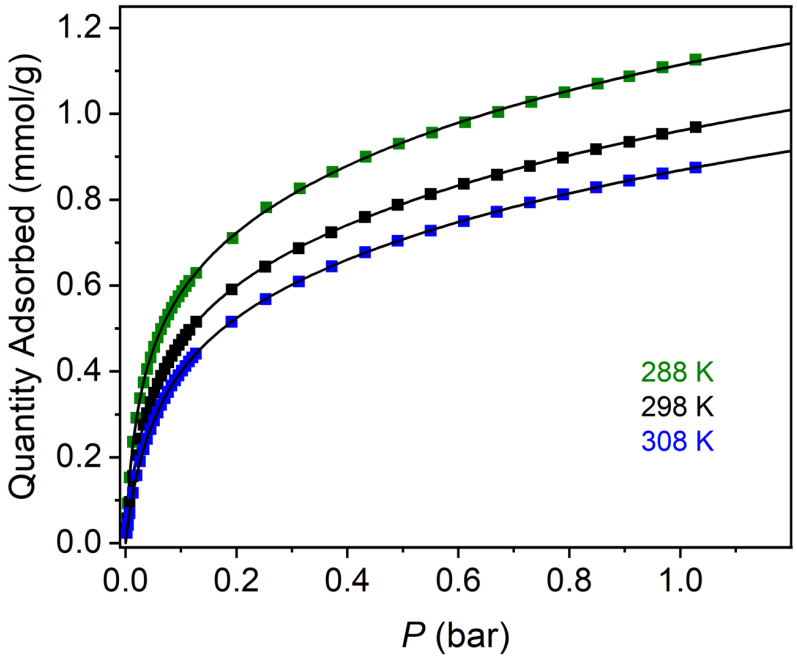

Figure S2.51. Pure component isotherm data for ethylene adsorption in (tc4a)Fe(btc). Experimental data are plotted as closed circles for isotherms measured at 288 K (green), 298 K (black), and 308 K (blue). The black lines are the respective dual-site Langmuir-Freundlich fits using the parameters in Table S2.11.

Table S2.11.

	288 K	**298 K**	**308 K**
$q_{sat,1}$ (mmol/g)	1.618320	1.388250	1.038570
b_1 (bar)	0.687870	0.483450	0.548500
v_1	0.664350	0.782730	0.902070
$q_{sat,2}$ (mmol/g)	0.467320	0.534900	0.535950
b_2 (bar)	36.486940	19.066430	14.154210
v_2	0.961200	0.939470	0.937800

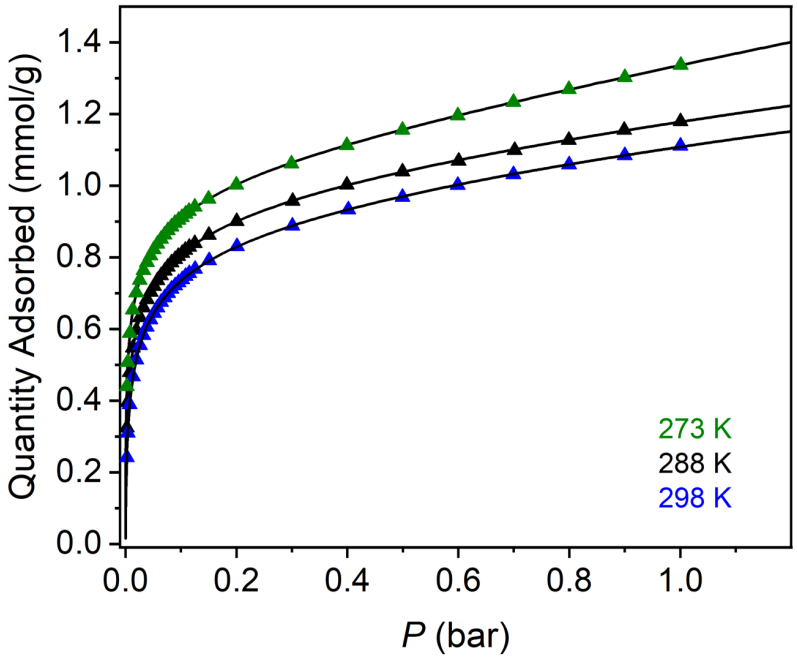

Figure S2.52. Pure component isotherm data for propane adsorption in (tc4a)Fe(btc). Experimental data are plotted as closed triangles for isotherms measured at 273 K (green), 288 K (black), and 298 K (blue). The black lines are the respective dual-site Langmuir-Freundlich fits using the parameters in Table S2.12.

Table S2.12.

	273 K	**288 K**	**298 K**
$q_{sat,1}$ (mmol/g)	1.32863	1.06177	100
b_1 (bar)	4.73844	7.68582	0.00327
v_1	0.3683	0.46556	0.60612
$q_{sat,2}$ (mmol/g)	49.99998	50	0.84238
b_2 (bar)	0.0048	0.00479	12.98292
v_2	1.09002	0.7874	0.57225

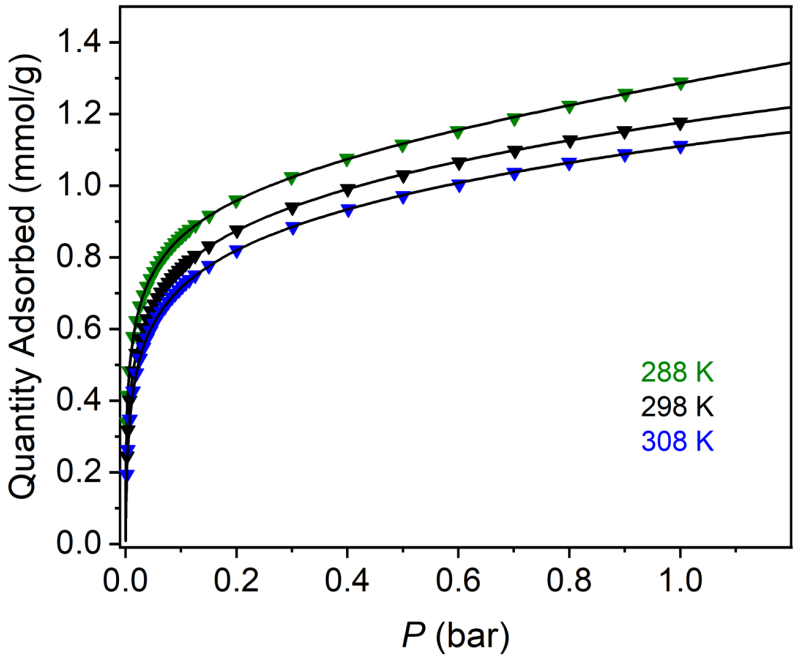

Figure S2.53. Pure component isotherm data for propylene adsorption in (tc4a)Fe(btc). Experimental data are plotted as inverted triangles for isotherms measured at 288 K (green), 298 K (black), and 308 K (blue). The black lines are the respective dual-site Langmuir-Freundlich fits using the parameters in Table S2.12.

Table S2.13.

	288 K	**298 K**	**308 K**
$q_{sat,1}$ (mmol/g)	100	11.80522	2.78926
b_1 (bar)	0.00255	0.04593	0.22709
v_1	0.913	0.42058	0.46625
$q_{sat,2}$ (mmol/g)	1.19879	0.69311	0.6188
b_2 (bar)	6.16115	18.41327	23.89066
v_2	0.44586	0.61536	0.68863

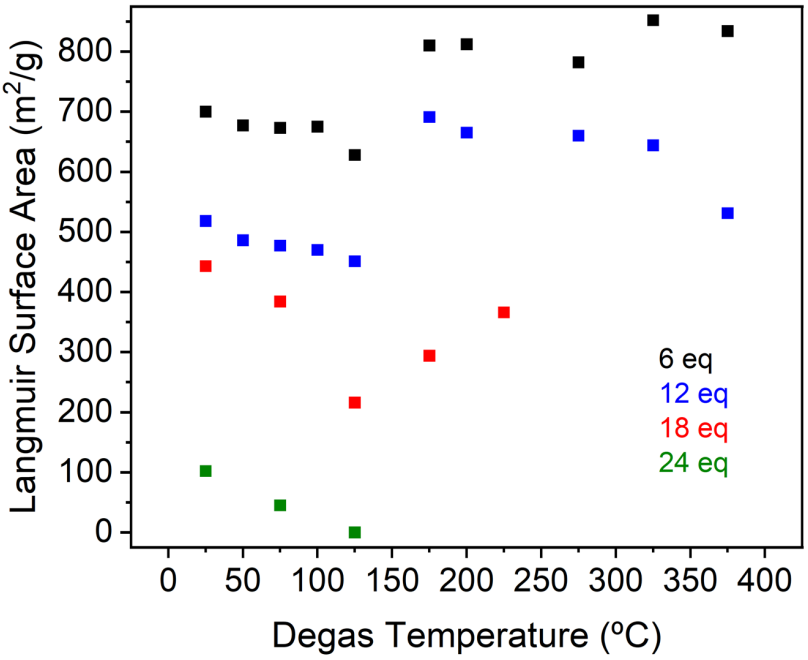

Figure S2.54. Plot showing Langmuir surface areas (N_2) for oxidized cages upon vacuum activation at different temperatures. For each point, samples were vacuum activated overnight and then Langmuir surface areas were determined. The same samples were activated at progressively higher temperatures to determine the optimal temperature for cage activation.

3. IR Spectra

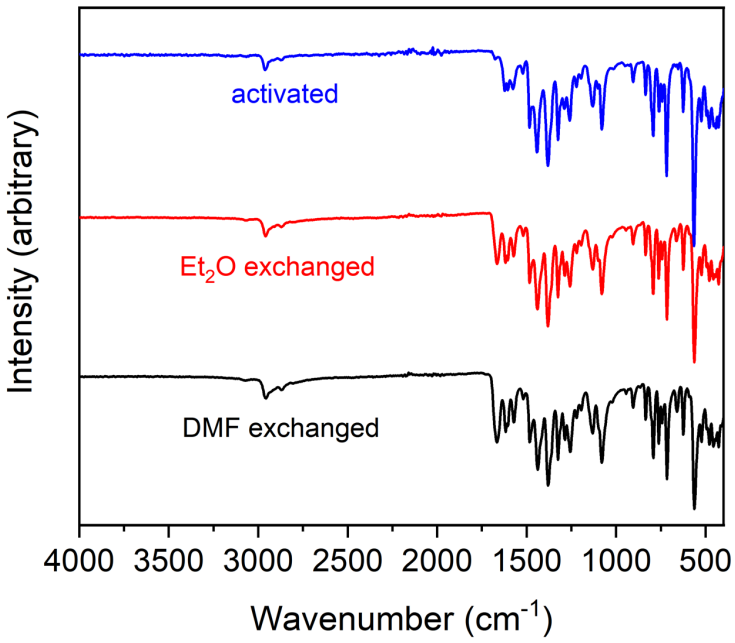

Figure S3.1. IR spectra of the (sc4a)Fe(btc) cage following DMF washes (black), solvent exchange with Et_2O (red), and vacuum activation at 175 ºC (blue).

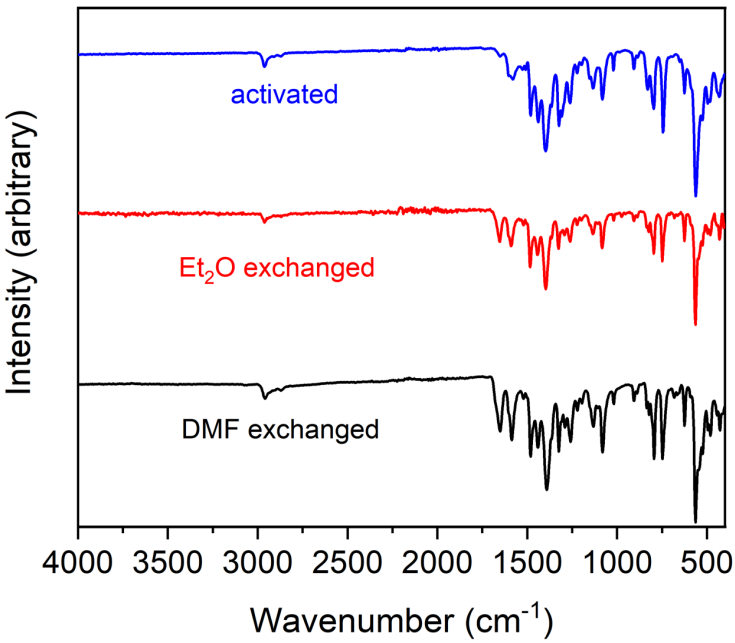

Figure S3.2. IR spectra of the (sc4a)Fe(bdc) cage following DMF washes (black), solvent exchange with Et_2O (red), and vacuum activation at 175 ºC (blue).

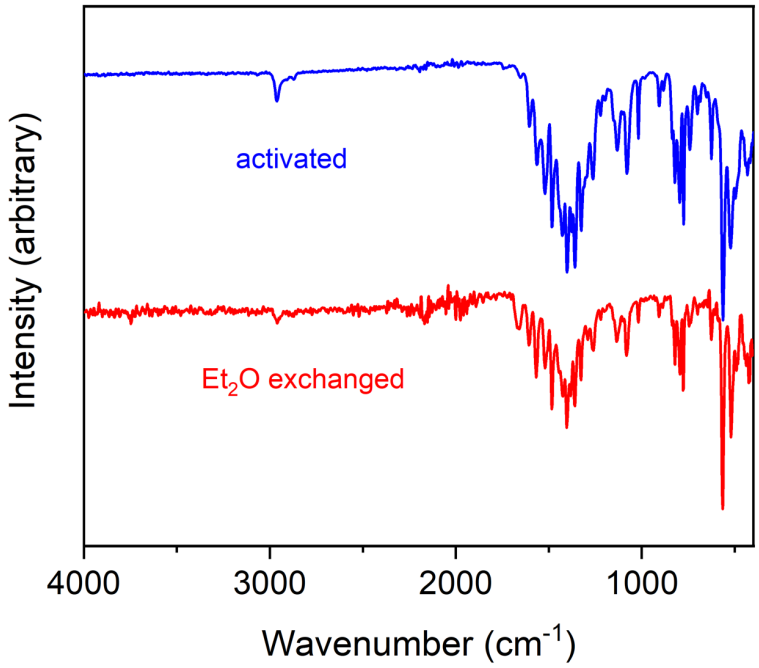

Figure S3.3. IR spectra of (sc4a)Fe(tatb) cage collected following solvent exchange with Et_2O (red) and vacuum activation at 125 ºC (blue).

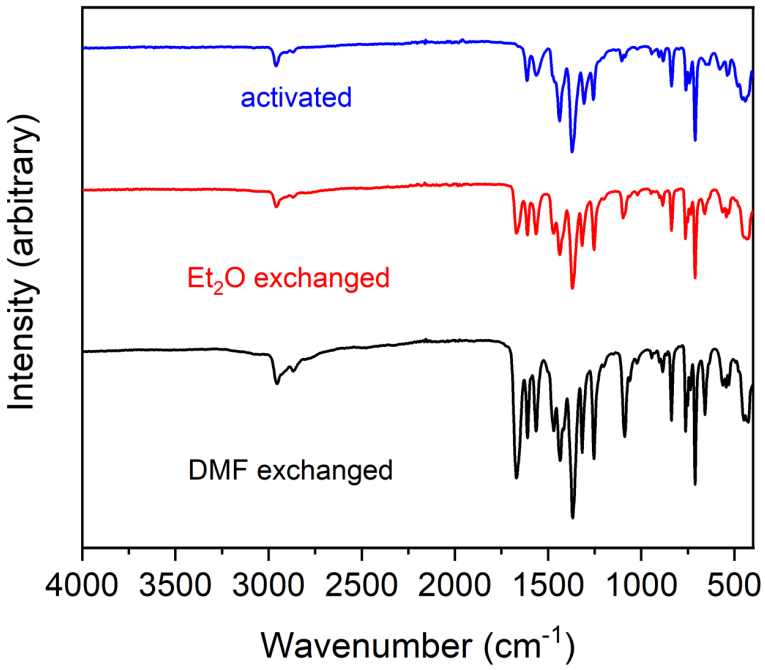

Figure S3.4. IR spectra of the (tc4a)Fe(btc) cage following DMF washes (black), solvent exchange with Et_2O (red), and vacuum activation at 200 ºC (blue).

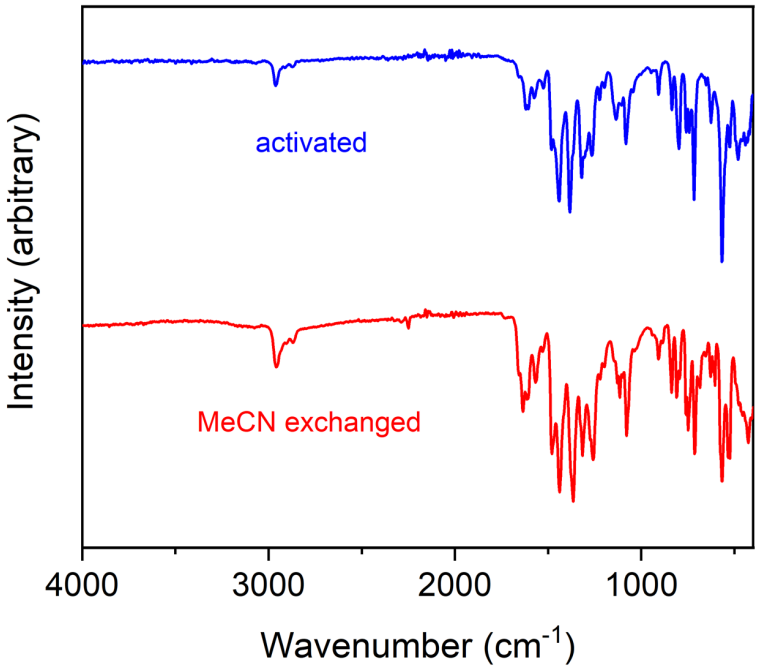

Figure S3.5. IR spectra of (sc4a)Fe(btc) cage upon treatment with 6 equiv. of magic blue following MeCN washes (red) and vacuum activation at 175 ºC (blue).

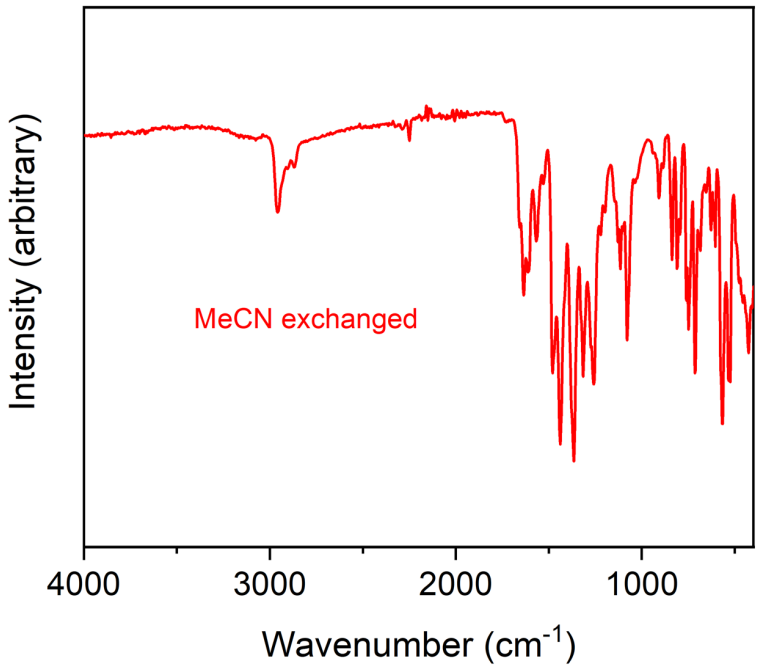

Figure S3.6. IR spectra of (sc4a)Fe(btc) cage upon treatment with 12 equiv. of magic blue following MeCN washes (red) and vacuum activation at 175 ºC (blue).

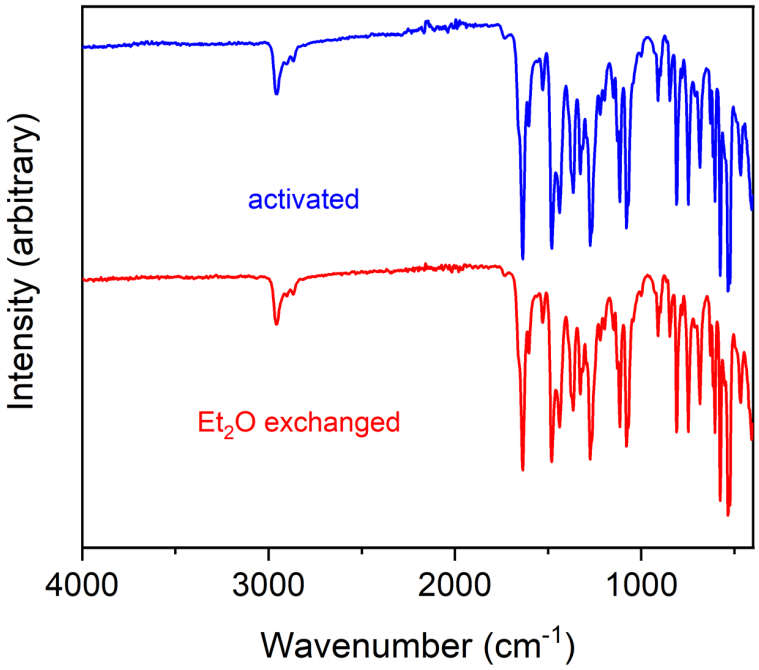

Figure S3.7. IR spectra of (sc4a)Fe(btc) cage upon treatment with 18 equiv. of magic blue following solvent exchange with Et_2O (black) and vacuum activation at room temperature (red).

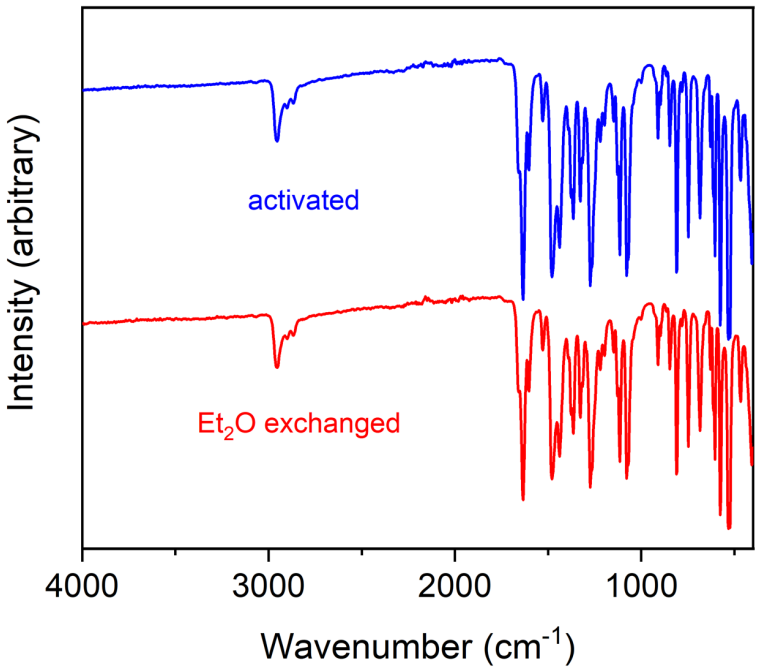

Figure S3.8. IR spectra of (sc4a)Fe(btc) cage upon treatment with 24 equiv. of magic blue following solvent exchange with Et_2O (black) and vacuum activation at room temperature (red).

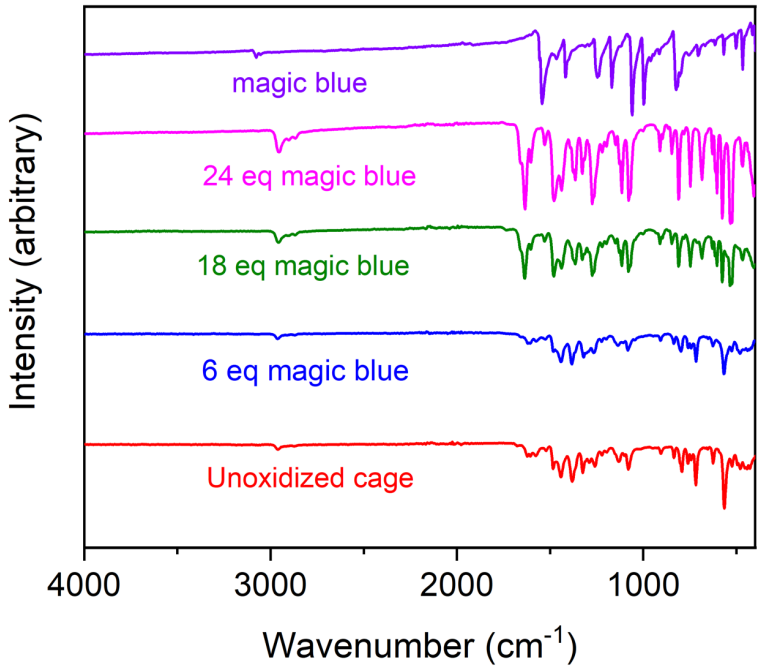

Figure S3.9. IR spectra of activated (sc4a)Fe(btc) cages over accessed formal oxidation states and magic blue.

4. Mössbauer Spectra

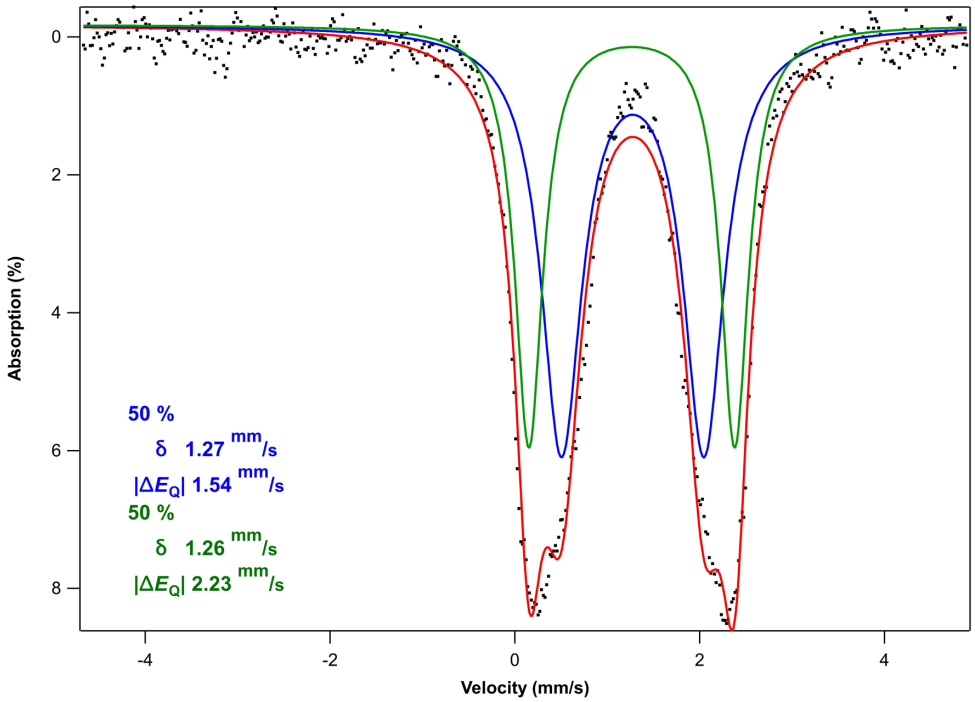

Figure S4.1. Mössbauer spectrum of the (sc4a)Fe(btc) cage.

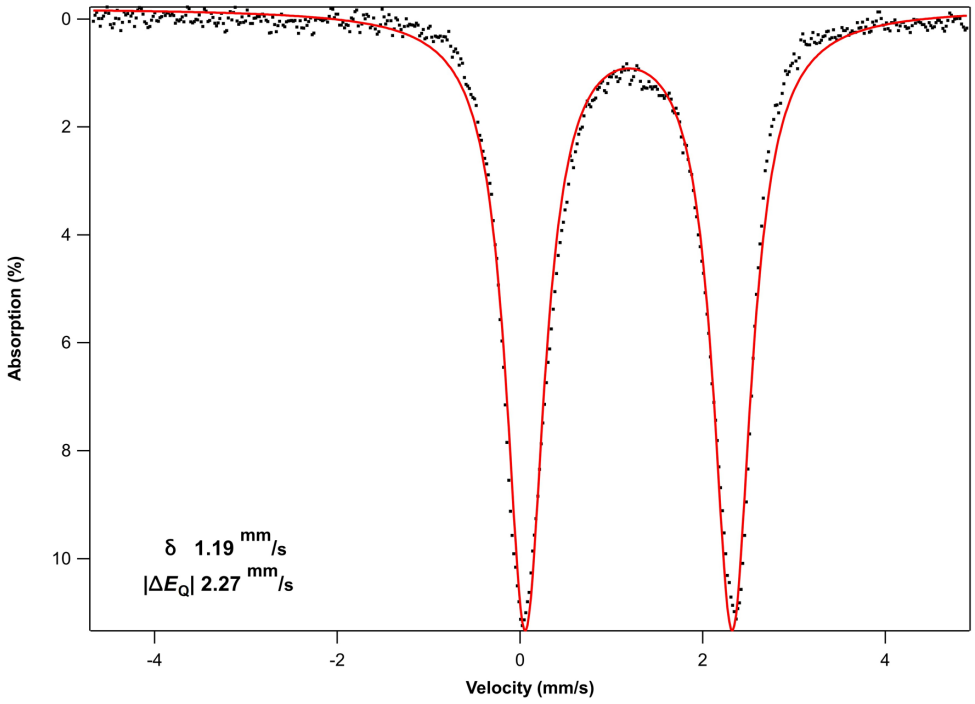

Figure S4.2. Mössbauer spectrum of the (tc4a)Fe(btc) cage.

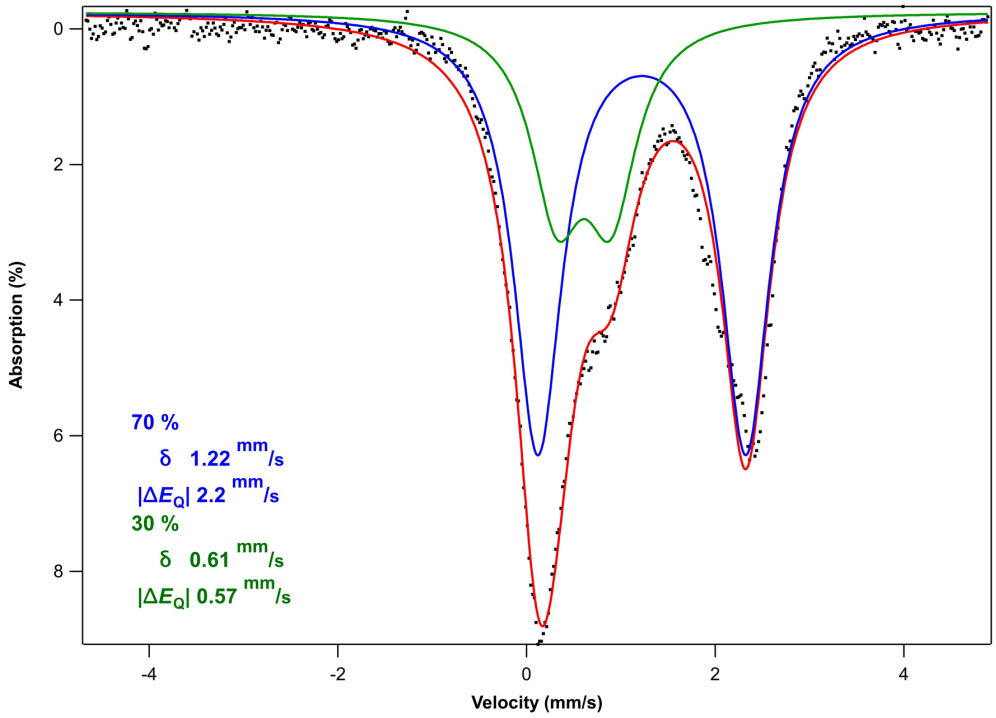

Figure S4.3. Mössbauer spectrum of one sample of the (sc4a)Fe(bdc) cage.

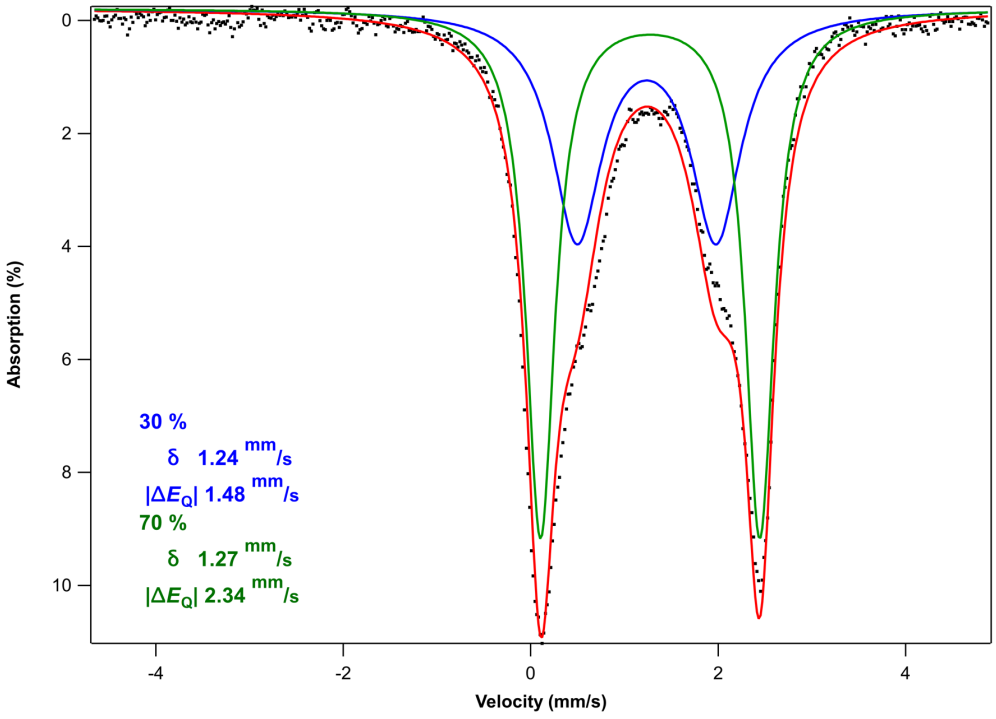

Figure S4.4. Mössbauer spectrum of a second sample of the (sc4a)Fe(bdc) cage.

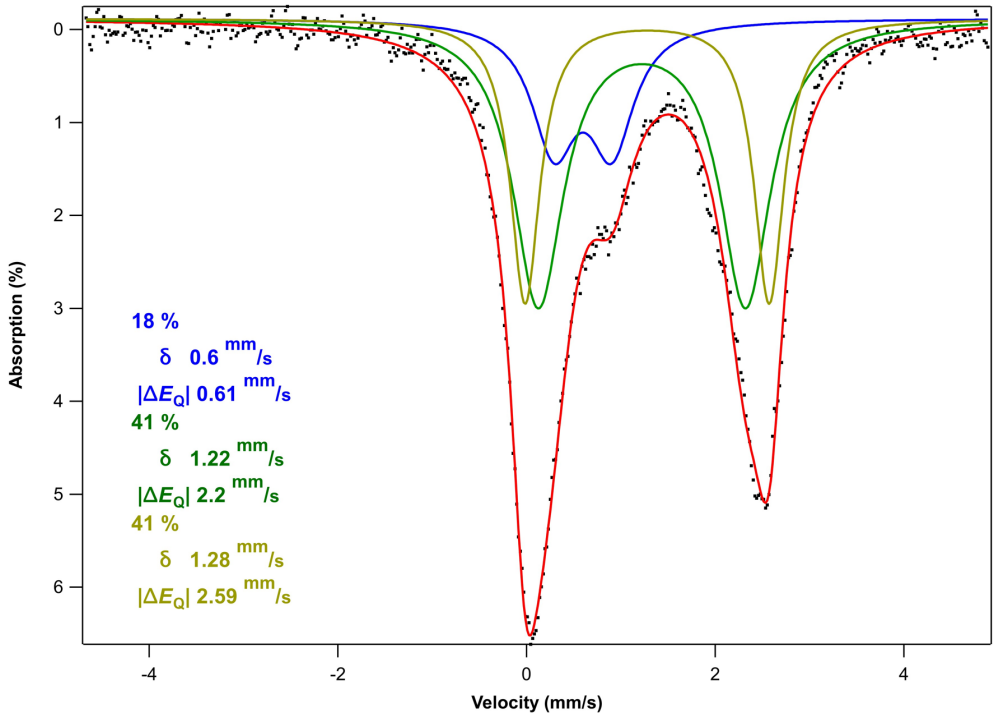

Figure S4.5. Mössbauer spectrum of the (sc4a)Fe(tatb) cage.

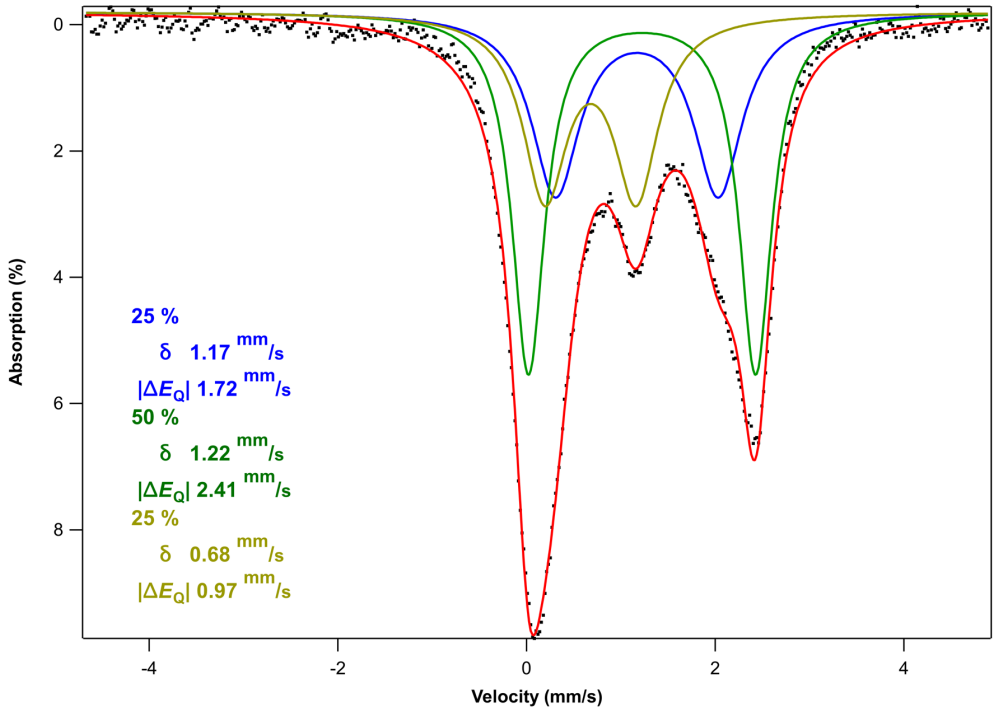

Figure S4.6. Mössbauer spectrum of the activated (sc4a)Fe(btc) cage following exposure to O_2.

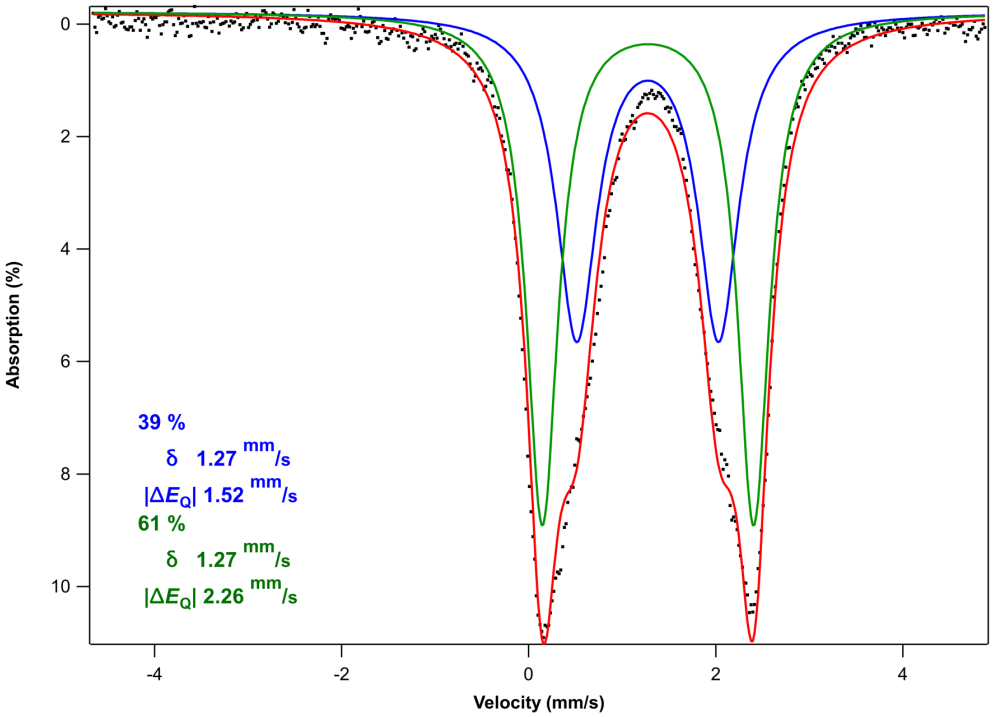

Figure S4.7. Mössbauer spectrum of the Et_2O exchanged (sc4a)Fe(btc) cage following prolonged storage in air.

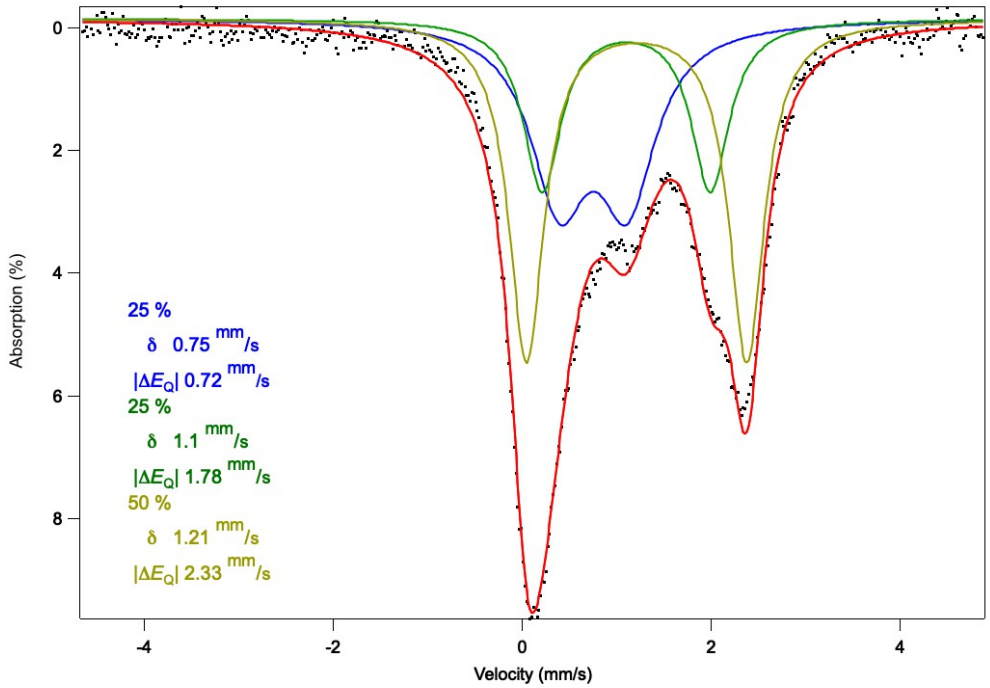

Figure S4.8. Mössbauer spectrum of the (sc4a)Fe(btc) cage when treated with 6 equiv. of magic blue.

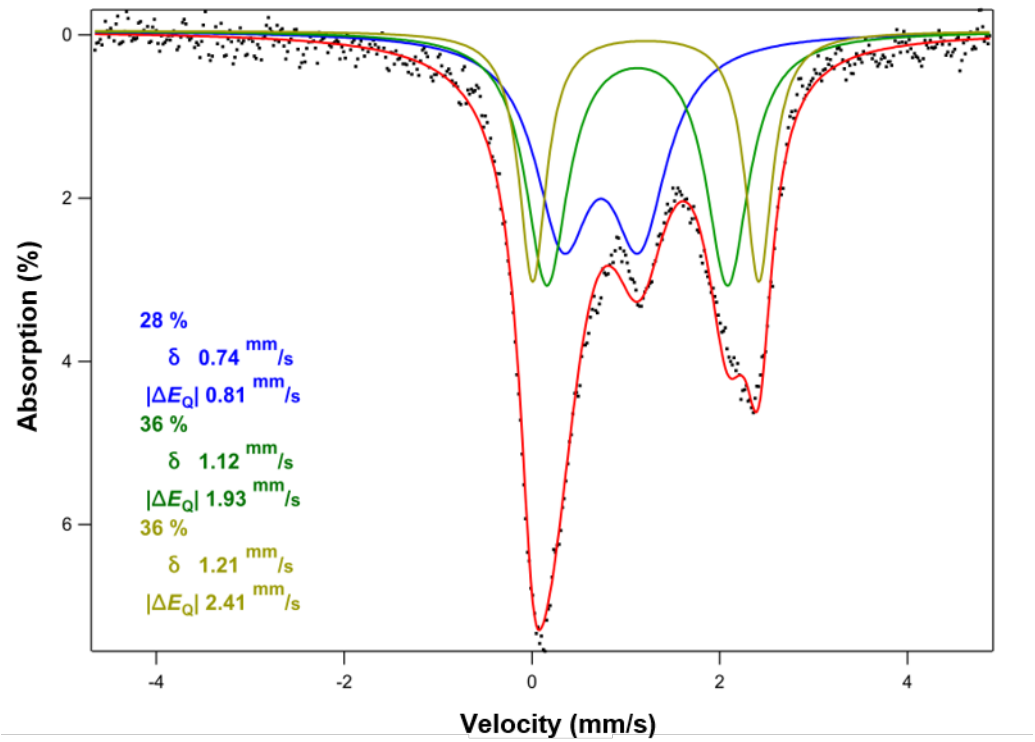

Figure S4.9. Mössbauer spectrum of the (sc4a)Fe(btc) cage when treated with 12 equiv. of magic blue.

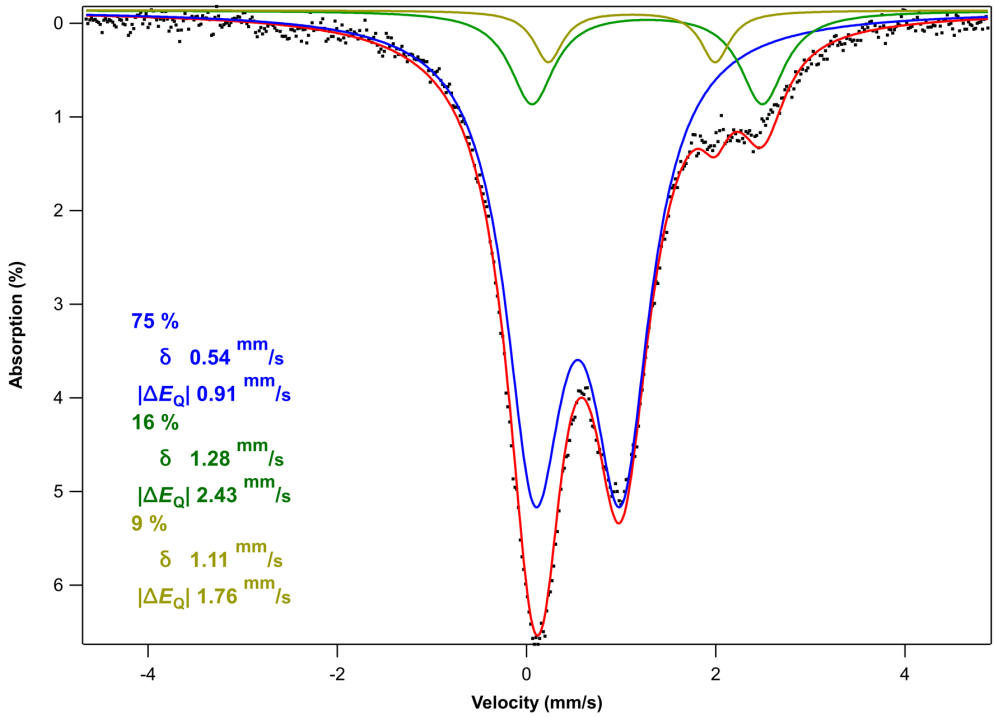

Figure S4.10. Mössbauer spectrum of the (sc4a)Fe(btc) cage when treated with 18 equiv. of magic blue.

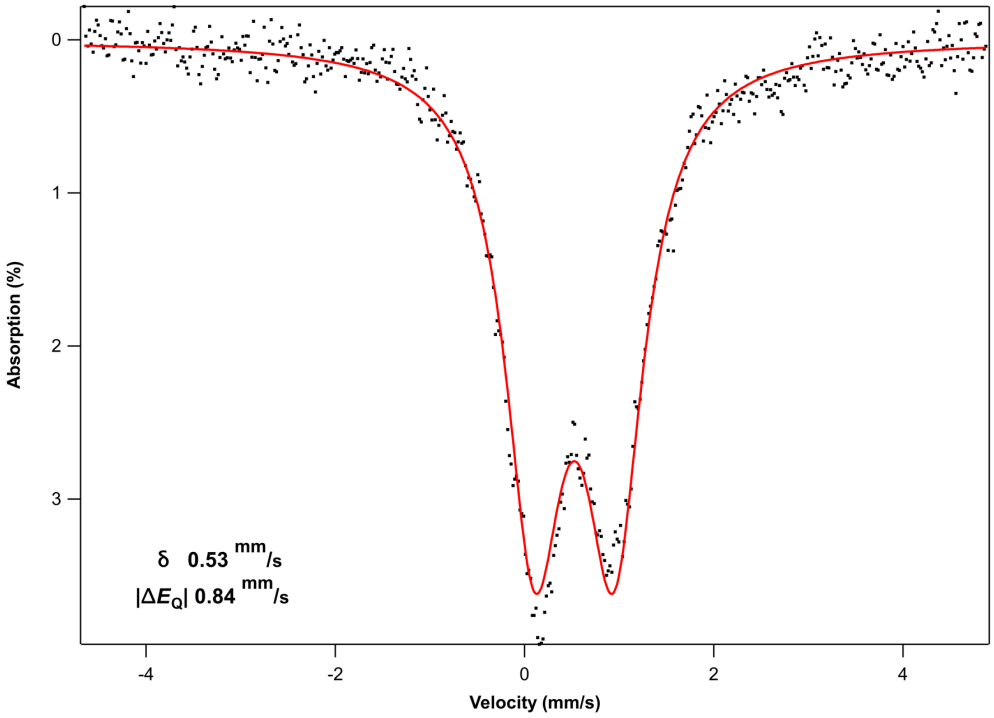

Figure S4.11. Mössbauer spectrum of the (sc4a)Fe(btc) cage when treated with 24 equiv. of magic blue.

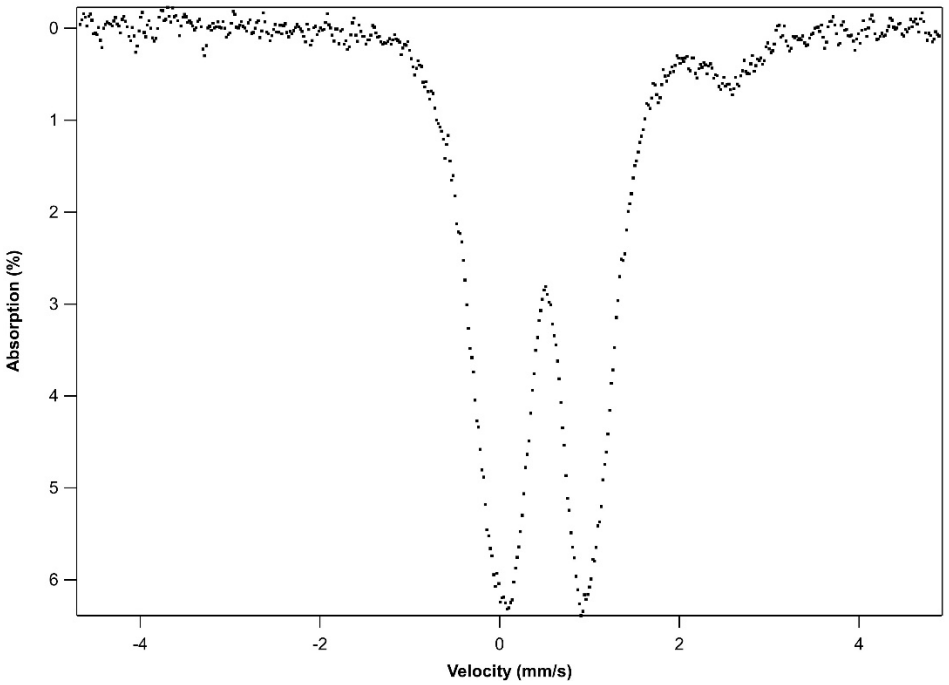

Figure S4.12. Mössbauer spectrum of as synthesized PCN-9 (Fe). The observed spectrum is similar to the previously published spectrum for this material prepared through an independent synthetic route.[8]

(8) S. Ma, D. Yuan, J.-S. Chang and H.-C. Zhou, *Inorg. Chem.*, 2009, **48**, 5398-5402.

5. Thermogravimetric Analysis

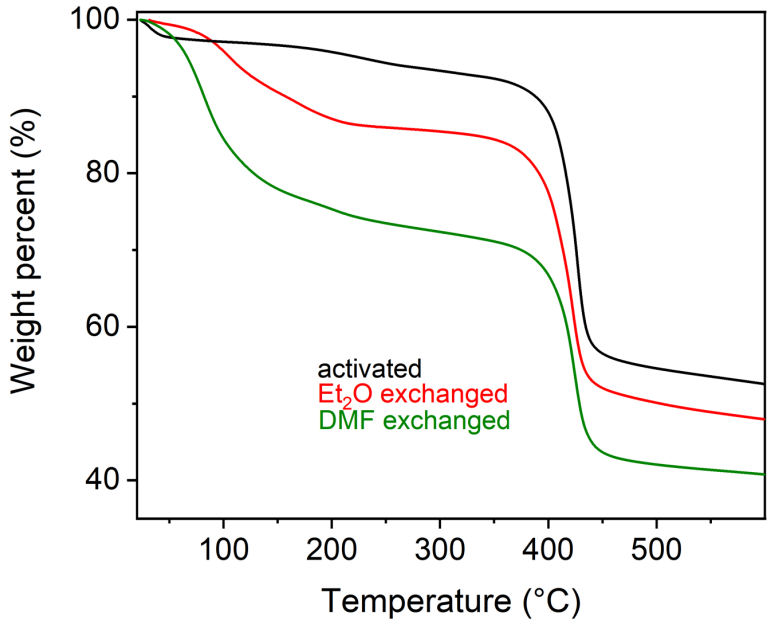

Figure S5.1. TGA of (sc4a)Fe(btc) cage following DMF washes (green), Et_2O exchange (red), and vacuum activation at 175 ºC (black).

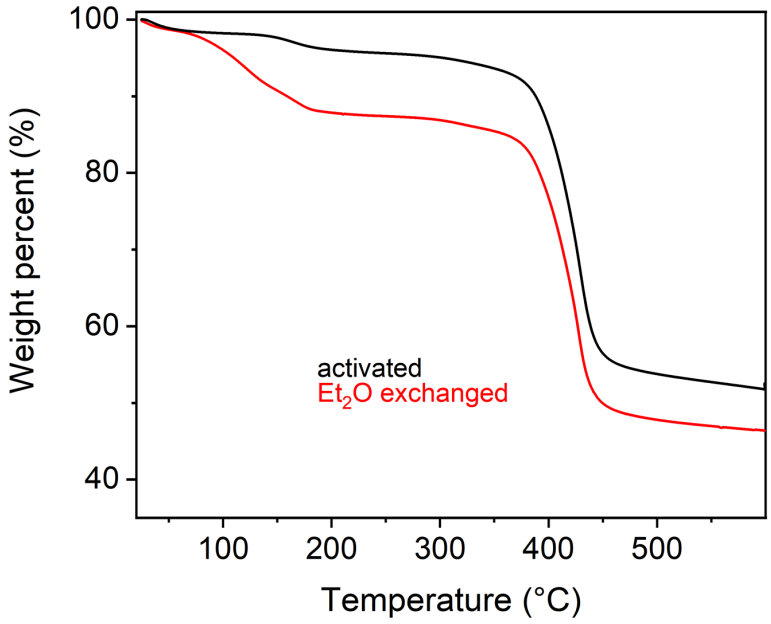

Figure S5.2. TGA of (sc4a)Fe(bdc) cage following Et_2O exchange (red), and vacuum activation at 175 ºC (black).

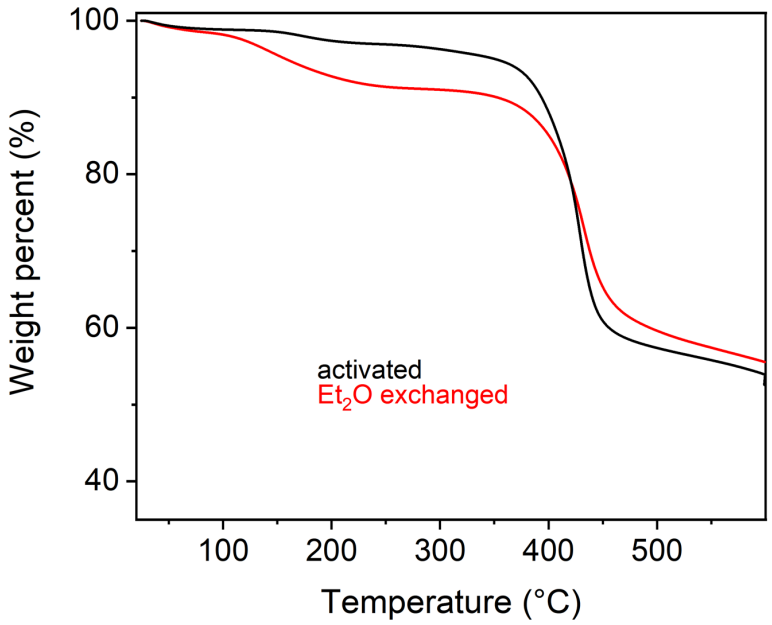

Figure S5.3. TGA of (sc4a)Fe(tatb) cage following Et_2O exchange (red), and vacuum activation at 125 ºC (black).

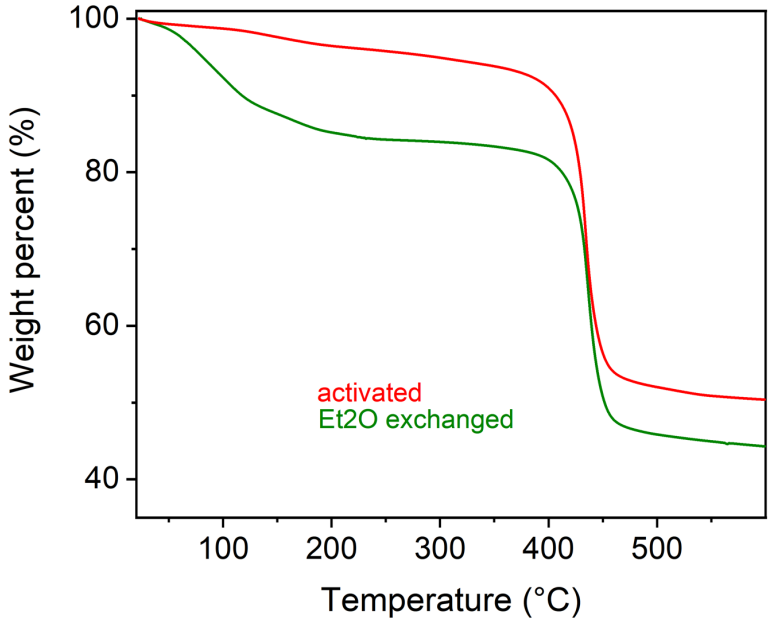

Figure S5.4. TGA of (tc4a)Fe(btc) cage following Et_2O exchange (green), and vacuum activation at 200 ºC (red).

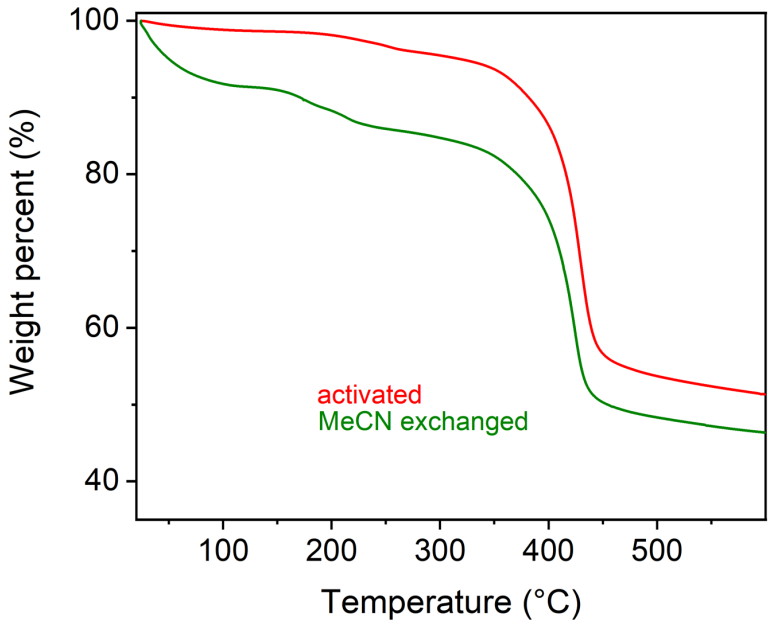

Figure S5.5. TGA of (sc4a)Fe(btc) cage upon treatment with 6 equiv. of magic blue following MeCN washes (green) and vacuum activation at 175 ºC (red).

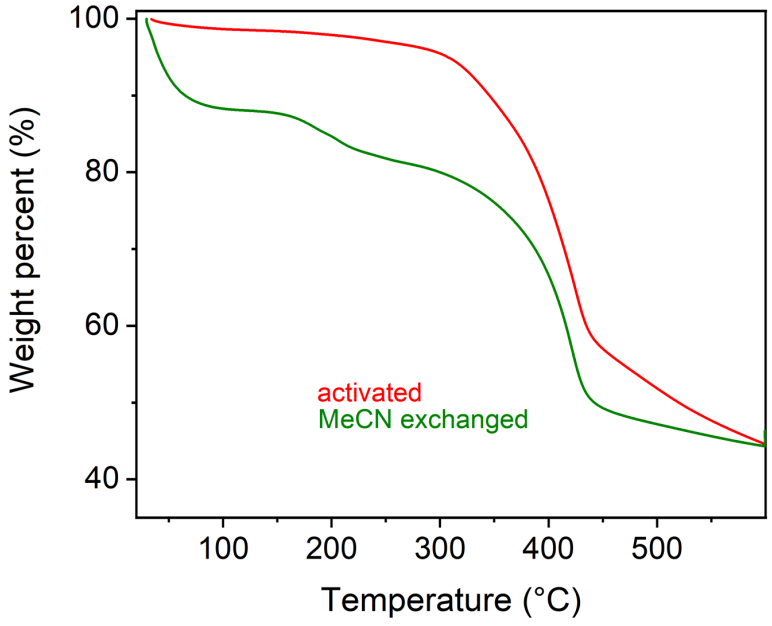

Figure S5.6. TGA of (sc4a)Fe(btc) cage upon treatment with 12 equiv. of magic blue following MeCN washes (green) and vacuum activation at 175 ºC (red).

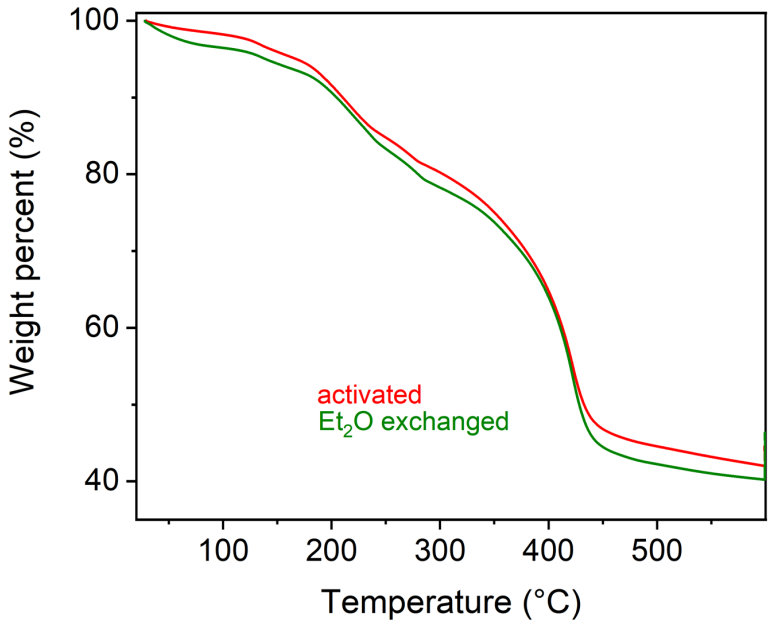

Figure S5.7. TGA of (sc4a)Fe(btc) cage upon treatment with 18 equiv. of magic blue following Et_2O exchange (green) and vacuum activation at room temperature (red).

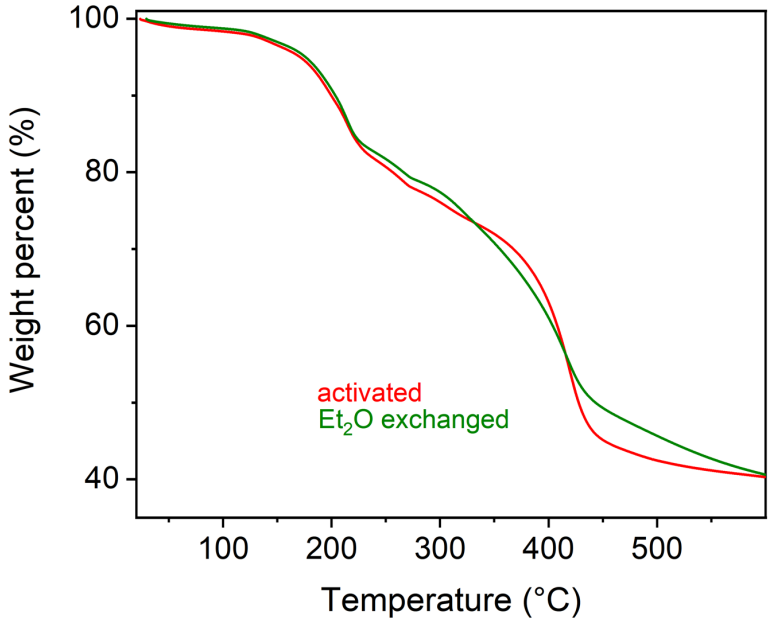

Figure S5.8. TGA of (sc4a)Fe(btc) cage upon treatment with 24 equiv. of magic blue following Et_2O exchange (green) and vacuum activation at room temperature (red).

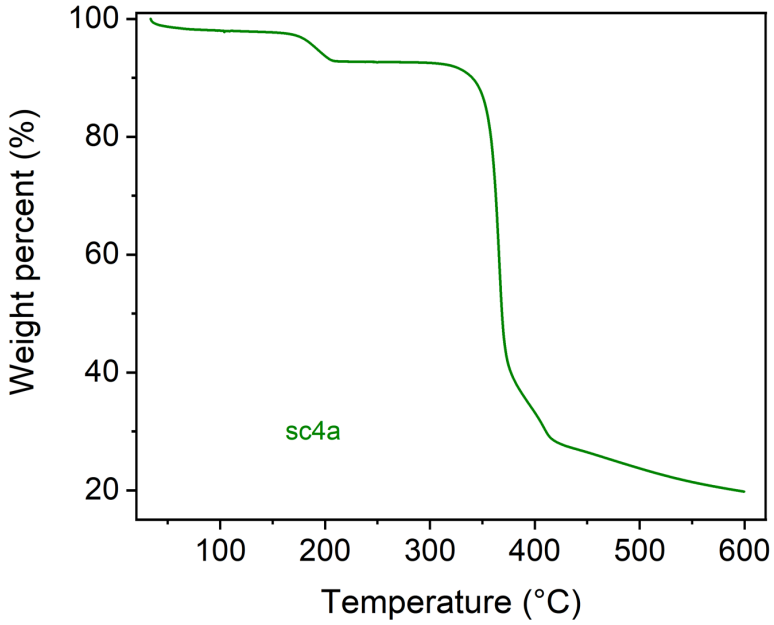

Figure S5.9. TGA of sc4a ligand.

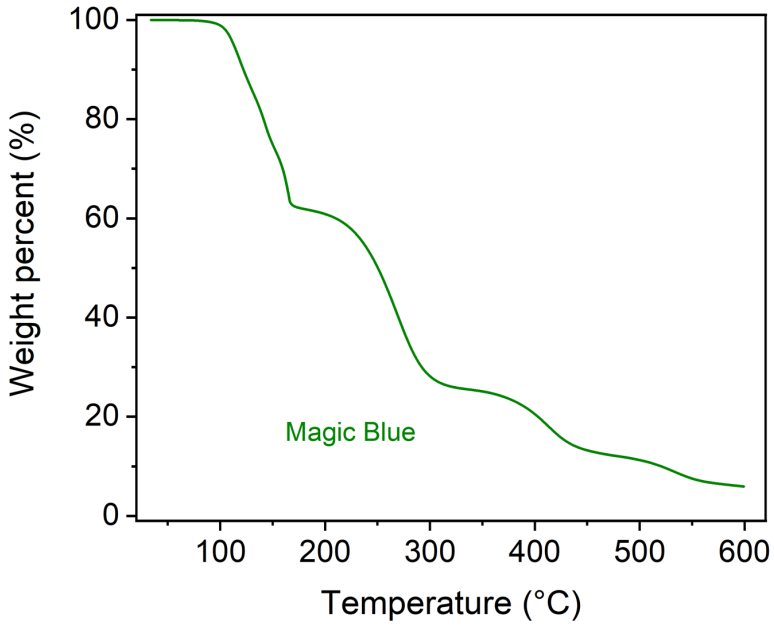

Figure S5.10. TGA of magic blue ($[N(4\text{-}BrC_6H_4)_3][SbCl_6]$).

6. Powder X-Ray Diffraction Patterns

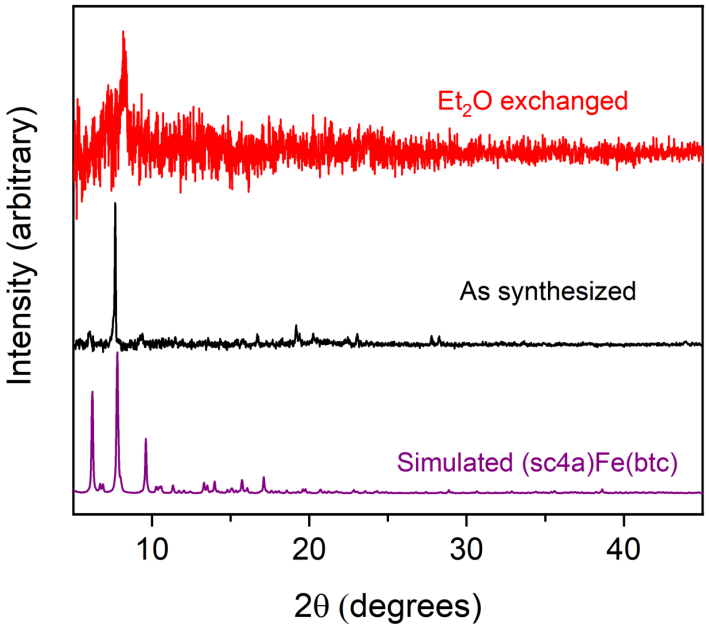

Figure S6.1. Powder XRD patterns simulated for the (sc4a)Fe(btc) cage (purple), as well as the experimental patterns for the as synthesized cage (black) and the Et_2O exchanged cage (red).

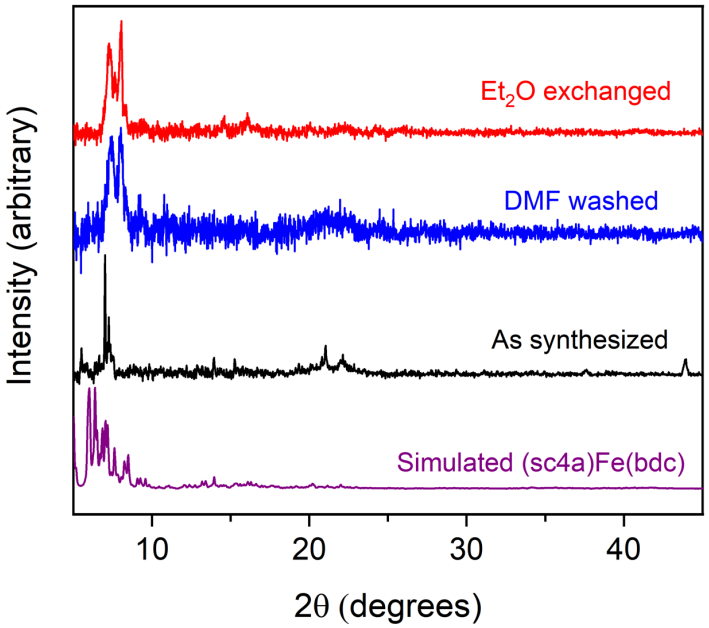

Figure S6.2. Powder XRD patterns simulated for the (sc4a)Fe(bdc) cage (purple), as well as the experimental patterns for the as synthesized cage (black), the DMF washed cage (blue), and the Et_2O exchanged cage (red).

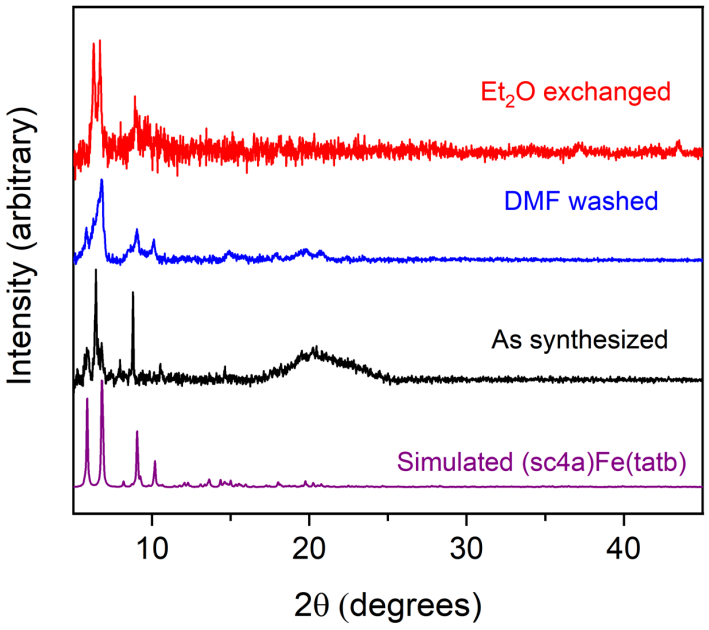

Figure S6.3. Powder XRD patterns simulated for the (sc4a)Fe(tatb) cage (purple), as well as the experimental patterns for the as synthesized cage (black), the DMF washed cage (blue), and the Et_2O exchanged cage (red).

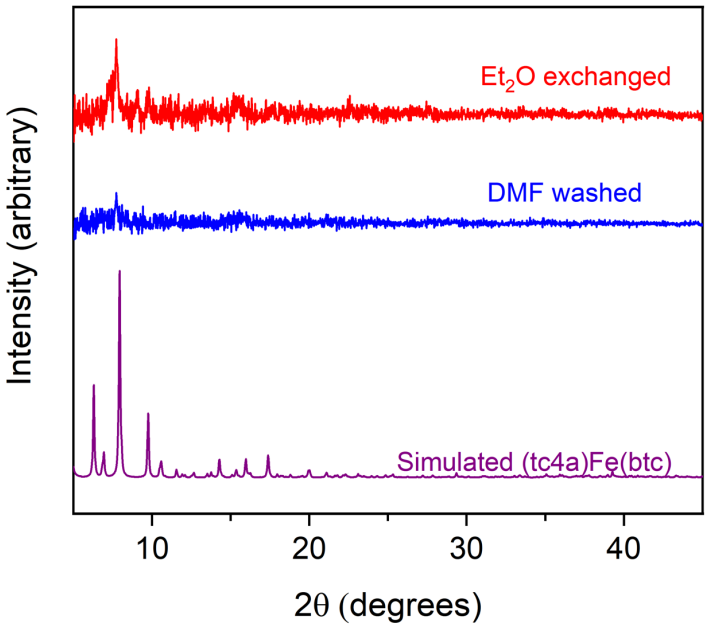

Figure S6.4. Powder XRD patterns simulated for the (tc4a)Fe(btc) cage (purple), as well as the experimental patterns for the DMF washed cage (blue) and the Et_2O exchanged cage (red).

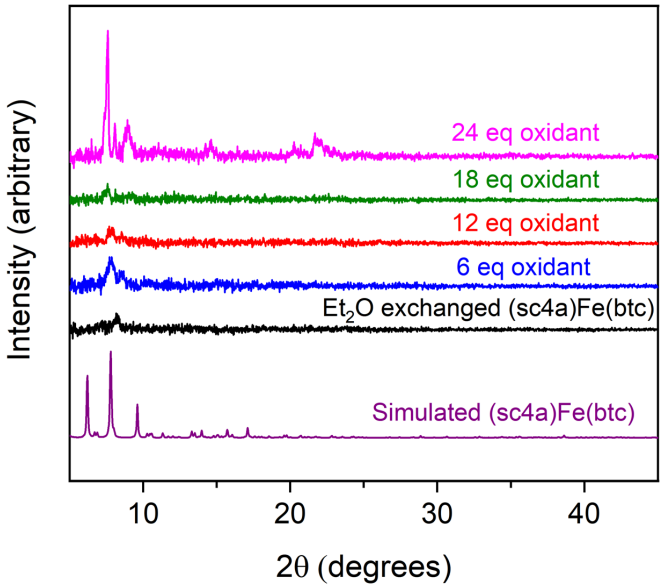

Figure S6.5. Powder XRD patterns simulated for the (sc4a)Fe(btc) cage (purple), as well as the experimental patterns for the Et_2O exchanged cage (black) and the materials generated upon treatment with 6 (blue), 12 (red), 18 (green), and 24 equiv. (pink) of magic blue.

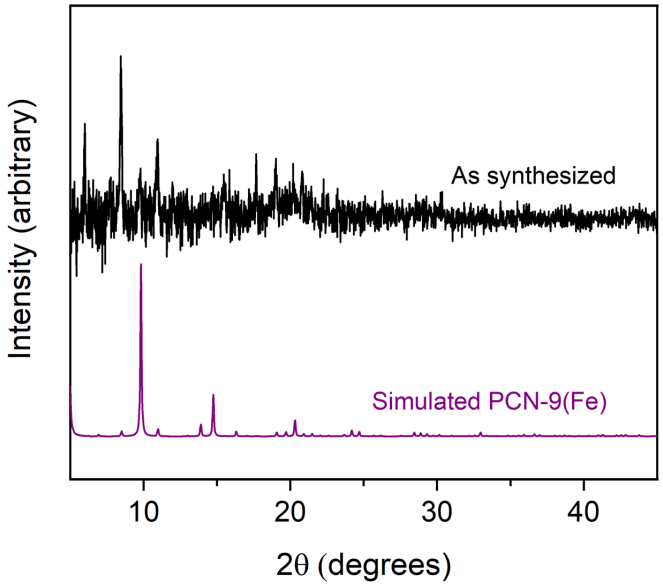

Figure S6.6. Powder XRD patterns simulated for the published structure of PCN-9 (Fe) (purple) and an experimental pattern for the as synthesized MOF (black). The experimental pattern is similar to the experimental pattern reported for PCN-9 (Co), neither of which match well with the simulated pattern.[9,10]

(9) S. Ma, D. Yuan, J.-S. Chang and H.-C. Zhou, *Inorg. Chem.*, 2009, **48**, 5398-5402.
(10) S. Ma and H.-C. Zhou, *J. Am. Chem. Soc.*, 2006, **128**, 11734-11735.

7. X-Ray Structures

	(sc4a)Fe(OAc)	(sc4a)Fe(btc)	(sc4a)Fe(bdc)	(sc4a)Fe(tatb)	(tc4a)Fe(btc)
Crystal System	Monoclinic	Tetragonal	Monoclinic	Rhombohedral	Tetragonal
Formula	$C_{55}H_{80}Fe_4NO_{23}S_4$	$C_{312}H_{288}Cl_6Fe_{24}O_{120}S_{24}$	$C_{336}H_{312}Cl_{1.3}Fe_{24}O_{124.7}S_{24}$	$C_{432}H_{360}Cl_6Fe_{24}N_{24}O_{120}S_{24}$	$C_{324}H_{316}C_{16}Fe_{24}N_4O_{76}S_{24}$
Formula weight (g/mol)	1474.84	8279.95	8501.01	10129.79	7804.33
Space group	C 2/m	I 4/m	P 21/c	R-3	I 4/m
a (Å)	38.135(7)	26.3817(4)	50.406(4)	30.082(7)	25.8237(8)
b (Å)	15.141(4)	26.3817(4)	26.7036(17)	30.082(7)	25.8237(8)
c (Å)	14.006(2)	44.1371(8)	54.416(3)	76.984(17)	43.8967(14)
α (deg)	90	90	90	90	90
β (deg)	101.009(7)	90	93.833	90	90
γ (deg)	90	90	90	120	90
Z	4	2	4	3	2
V (Å^3)	7938(3)	30719.2(11)	73081(8)	60331(30)	29273.1(16)
Indep. Reflections	5392	10497	43155	4213	14074
R (int)	0.0919	0.0378	0.1991		0.0867
R1	0.0540	0.0889	0.1139	0.1498	0.0630
wR2	0.1501	0.2701	0.3573	0.4577	0.1995
GOF	1.033	1.022	1.183	2.038	1.041

Refinement Details:

[(sc4a)Fe(OAc)$_4$(μ$_4$-OMe)][TMA]: The cluster co-crystallizes with one resolved MeOH molecule and a TMA countercation. One of the *t*-butyl residues of the sc4a ligand was modeled as disordered over two positions (52:49). Refinement of this disorder was aided by application of RIGU, SIMU, and SADI restraints as well as EADP constraints. One A-level checkcif alert is associated with relatively weak diffraction data for this cluster.

It is well-established that the disordered contents in the structures of highly porous materials such as metal-organic frameworks and molecular metal-organic polyhedra often result in weak diffraction data that are limited in coverage and resolution. As a result, it is common to have multiple restraints and constraints, incompletely identified moieties, and high residuals in the structural model.[11] Disordered solvent molecules in the pore void space could not reliably be refined and, as such, were treated using the application of SQUEEZE.

(sc4a)Fe(btc): Cage structure refinement was aided by the application of a SIMU restraint over all atoms. Refinement of one of the *t*-butyl residues was aided by application of SADI restraints with the central C-atom restrained to be coplanar with the attached aryl ring using a FLAT command. One A-level alert is associated with the weak diffraction data for this MOP.

(sc4a)Fe(bdc): Cage structure refinement was aided by the application of SIMU and RIGU restraints over all atoms. SADI restraints were applied to aid the refinement of the *t*-butyl residues. An additional SADI restraint and a DELU restraint was applied to aid in the refinement of the μ$_4$ atom, which was modeled as disordered between a Cl and a OH. Each of the six crystallographically distinct μ$_4$-positions was allowed to refine freely, with all positions refining to 75-82% O, with Cl accounting for the remaining fraction and

(11) Z. Perry, Y.-P. Chen, J. Bae, and H.-C. Zhou, *ACS Appl. Mater. Interfaces,* 2017, **9**, 28064-28068.

residual electron density. An additional DFIX command was applied to restrain the Fe-Cl distances. The largest six residual electron density peaks were located in a position such that the μ_4 groups might be OMe rather than OH groups, but attempts to fully refine such a model were unsuccessful. One A-level checkcif alert and four B-level checkcif alert are associated with the poor diffraction data.

(sc4a)Fe(tatb): Cage structure refinement was aided by the application of SIMU and RIGU restraints over all atoms. Refinement of the *t*-butyl groups was aided by application of SADI restraints. Refinement of tatb carboxylate residues was aided by the application of a SADI restraint on the C-O distances and a DFIX restraint on C-C distances. Three A-level and one B-level checkcif alerts are associated with poor quality of the diffraction data.

(tc4a)Fe(btc): One DMF molecule sitting in an external cavity of one of the calixarene ligands could be refined with the aid of SIMU and RIGU restraints. Refinement of the *t*-butyl residues was also aided by the application of SIMU and RIGU restraints. No A- or B-level checkcif alerts were noted for this cage.

Additional Structure Depictions

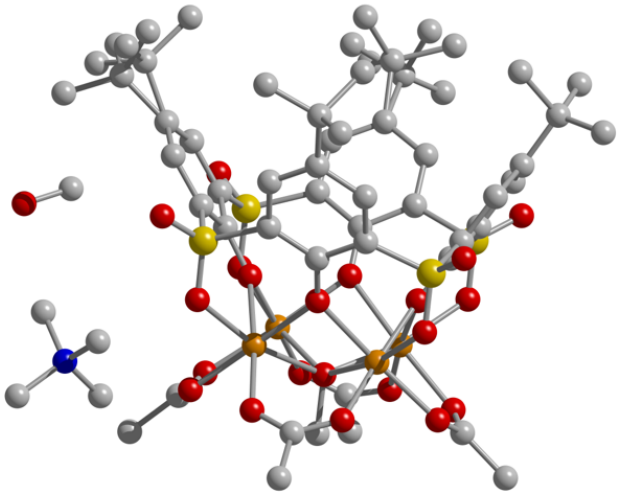

Figure S7.1. Full asymmetric unit of **[(sc4a)Fe(OAc)$_4$(μ_4-OMe)][TMA]** with hydrogen atoms omitted for clarity.

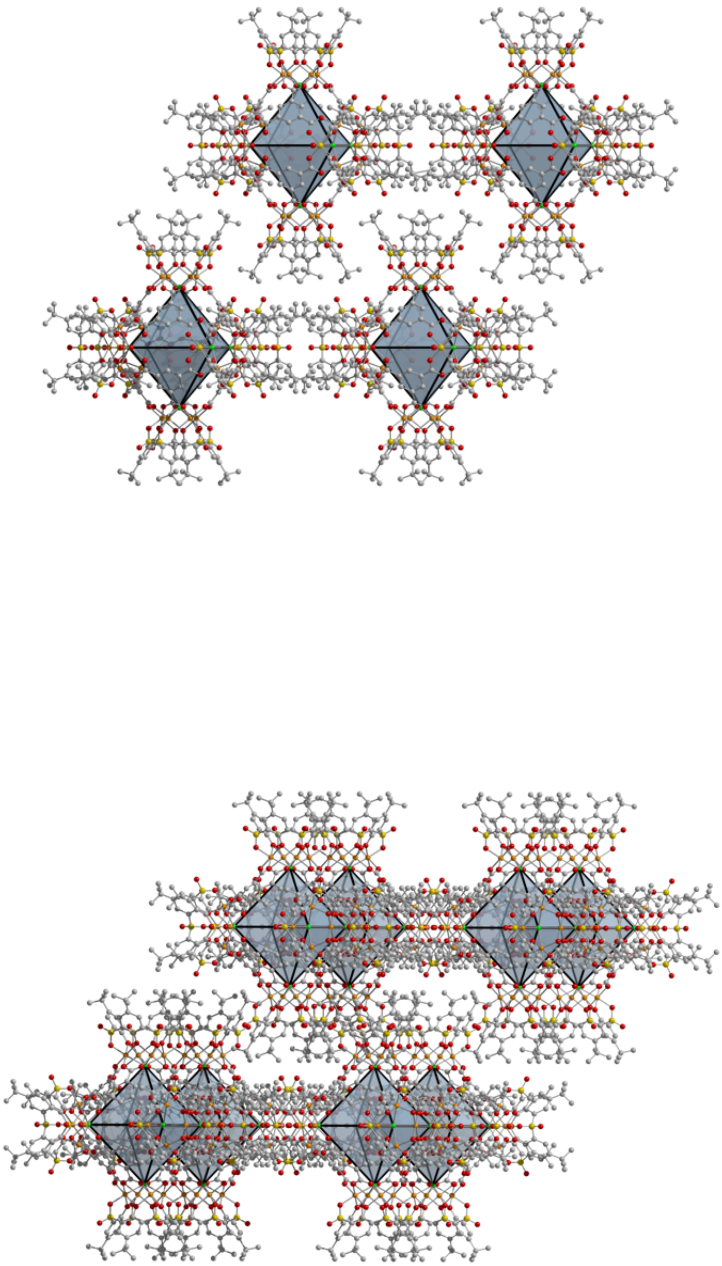

Figure S7.2. Solid state packing observed for the (sc4a)Fe(btc) cage viewed along the crystallographic b-axis (top) and slightly offset (bottom). The (tc4a)Fe(btc) cage crystallizes in the same space group with a near identical unit cell and packs in the same fashion.

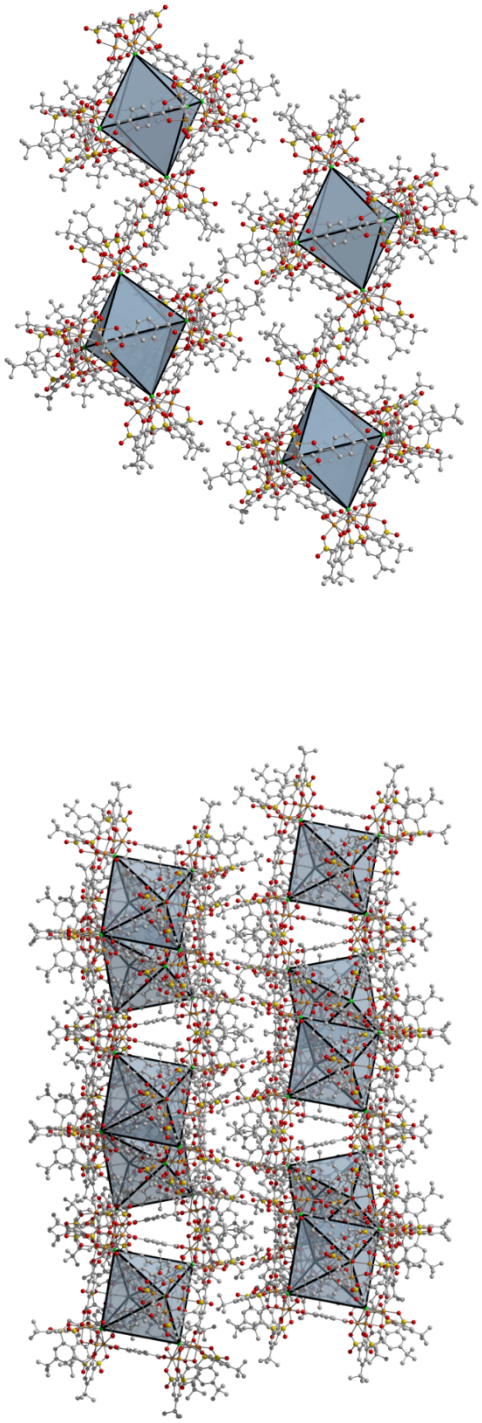

Figure S7.3. Two views of the solid state packing of cages in the structure of (sc4a)Fe(bdc).

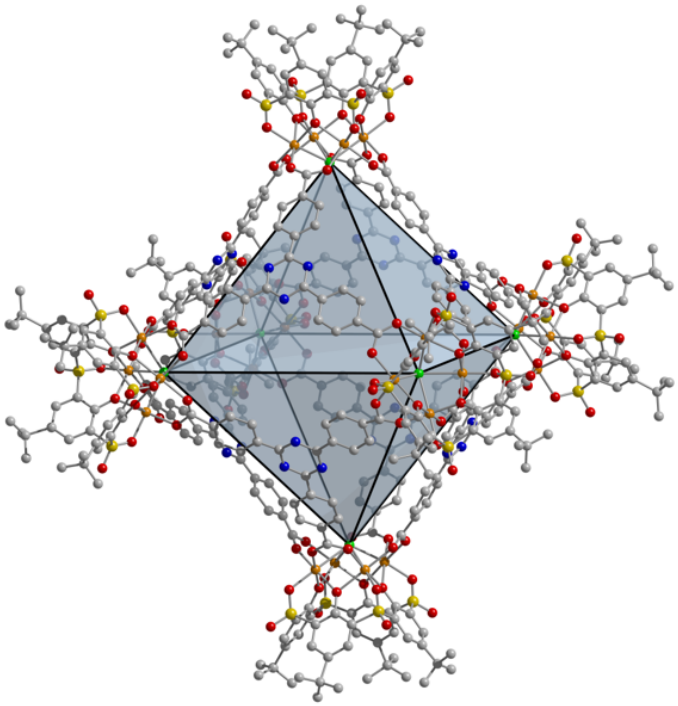

Figure S7.4. Solid-state structure of the (sc4a)Fe(tatb) cage.

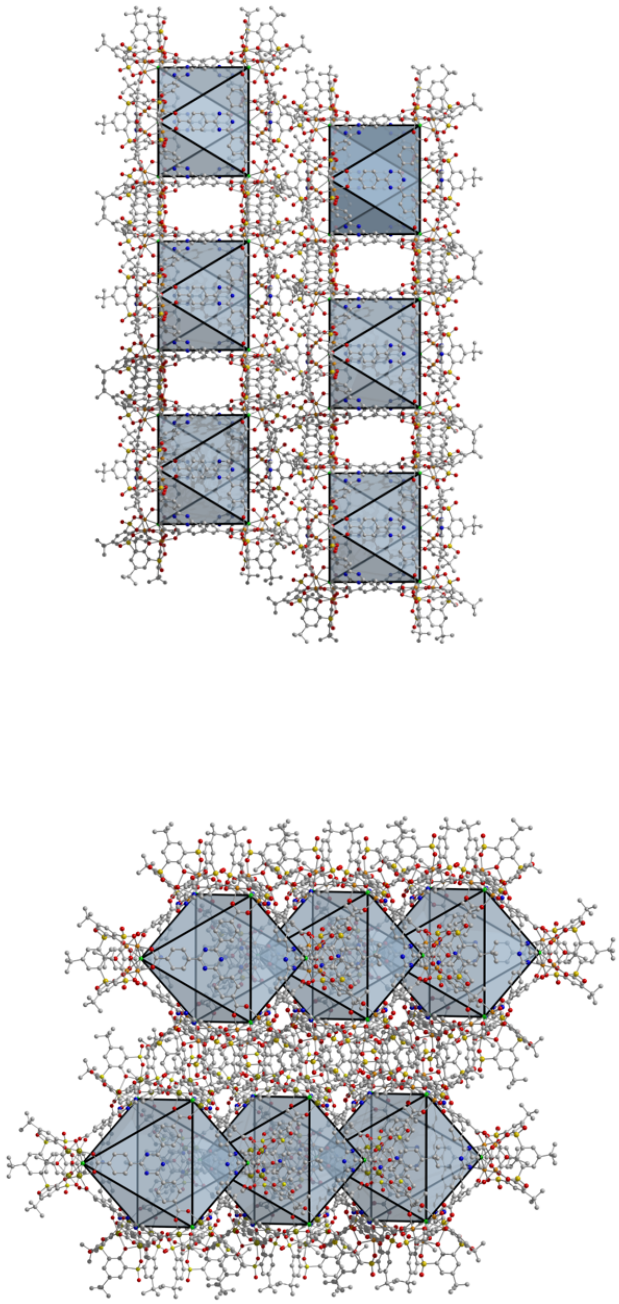

Figure S7.5. Solid state packing for the (sc4a)Fe(btc) cage viewed along the crystallographic b-axis (top) and an offset view (bottom).